Annu. Rev. Phys. Chem. 2001. 52:463–98

SPIN-½ AND BEYOND: A Perspective in Solid State NMR Spectroscopy

Lucio Frydman*
Department of Chemistry, University of Illinois at Chicago, 845 W. Taylor St., Rm 4500, Chicago, Illinois 60607; e-mail: lucio@uic.edu

Key Words spin interactions, high resolution NMR, quadrupolar nuclei, structural determinations

■ **Abstract** Novel applications of solid state nuclear magnetic resonance (NMR) to the study of small molecules, synthetic polymers, biological systems, and inorganic materials continue at an accelerated rate. Instrumental to this uninterrupted expansion has been an improved understanding of the chemical physics underlying NMR. Such deeper understanding has led to novel forms of controlling the various components that make up the spin interactions, which have in turn redefined the analytical capabilities of solid state NMR measurements. This review presents a perspective on the basic phenomena and manipulations that have made this progress possible and describes the new opportunities and challenges that are being opened in the realms of spin-½ and quadrupole nuclei spectroscopies.

INTRODUCTION

Although the foundations of nuclear magnetic resonance (NMR) were laid long ago (1), its scope and range of applications have remained in constant change through the decades (2–14). This progress has resulted from a better understanding of NMR's quantum principles, from new technical developments, and perhaps most importantly, from the unique opportunities provided by NMR itself. Indeed, NMR is in many ways any spectroscopist's dream, enabling nearly arbitrary manipulations of the interactions and the generation of unusually long-lived coherent states. It is thus not surprising that, when it comes to advancing the frontiers of spectroscopy, much new ground is broken first in NMR. In terms of applications, it is also not surprising that NMR could reach so deeply into such diverse realms as medical imaging, structural biology, analytical chemistry, and material sciences. In fact, the spectroscopic principles involved in the application of NMR to such disimilar disciplines are related to one another and in many instances find their

* Present address: Department of Chemical Physics, Weizmann Institute of Sciences, 76100 Rehovot, Israel

0066-426X/01/0601-0463$14.00

most challenging test ground in the topic treated by this article: the NMR of solids. A general discussion on solid state NMR seems justified by interesting physical ideas that have recently emerged in the area, by the new challenges and horizons that these new principles have revealed, and by the promising applications that these have opened up towards the characterization of a wide variety of solid materials. Because even modest coverage of all such recent developments would exceed the scope of an article (see 12–16 for excellent recent treatments of these topics), the objectives of this review are limited: to present a contemporary "stand-alone" perspective on the principles of solids NMR, and to exploit this background for introducing some of the latest developments in this area. The latter are described in mostly physical rather than mathematical terms in the hope of stressing their rationale, applications, and potential limitations.

SOLIDS NMR: Interactions and Spectra

NMR Interactions as Scalar Products Between Spin and Spatial Tensors

NMR is based on observing the oscillating signals that arise when an ensemble of nuclear spins is placed inside a strong static magnetic field B_o, and then taken away from equilibrium by the action of radiofrequency (*rf*) pulses. All NMR-active nuclides are characterized by a magnetic dipole moment μ, and therefore these time-dependent signals will be mostly governed by the spins' magnetic coupling to either external or internal fields. By virtue of the spins' quantum nature, these couplings are best represented by Hamiltonians, defining both the allowed energy levels and the spins' evolution in time (2, 3, 5). Under the sound assumption that fields can be represented by classical continuous functions, these operators take the general form $\mathcal{H}_\lambda = -\mu \cdot B_\lambda = -\gamma S \cdot B_\lambda$, where B_λ is a generic field, S is a spin's angular momentum, and γ is the nuclear magnetogyric constant.

Dominating NMR is the Zeeman interaction between spins and an external magnetic field B_o

$$\mathcal{H}_Z = -\gamma(S_x, S_y, S_z) \cdot (0, 0, B_o) = -\gamma B_o S_z = -\omega_o S_z, \qquad 1.$$

with a formally similar interaction representing the spins' coupling with the magnetic components of a transverse time-dependent field $B_{rf}(t)$. Although such Zeeman and *rf* couplings are essential for carrying out the NMR experiment, molecular information becomes available through the coupling of spins to locally generated magnetic fields. For instance, separation between inequivalent sites is promoted by the chemical shielding, reflecting the fields B_{ind} that are induced by electrons when a molecule is immersed inside B_o (1, 11). Owing to the anisotropic ease with which B_o can induce electronic currents, these fields are proportional to B_o in magnitude ($|B_{ind}| \approx 10^{-5} \cdot |B_o|$) but not necessarily in spatial direction;

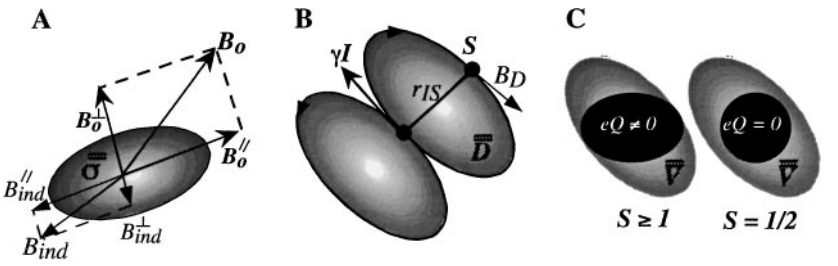

Figure 1 Tensorial nature of coupling tensors in solid state NMR. (*A*) Chemical shielding $\bar{\bar{\sigma}}$ and the origin of fields B_{ind}, deviating from B_o unless the latter is oriented along one of the spheroid's principal axes. (*B*) Idem for the *I-S* dipolar interaction. (*C*) Field gradient $\bar{\bar{V}}$ tensors and their ensuing electrostatic coupling with charged, nonspherical ($S \geq 1$) nuclei.

therefore, they require $3 \times 3\,\bar{\bar{\sigma}}$ tensors for their complete description (Figure 1*A*), and lead to a Hamiltonian $\mathcal{H}_{CS} = -\mu \cdot B_{ind} = \gamma S \cdot \bar{\bar{\sigma}} \cdot B_o$.[1]

Because nuclear magnetic dipoles not only couple to fields but also generate them, the NMR evolution of a spin *S* may be influenced by the fields arising from neighboring nuclei *I*. Once again these effects will be proportional to the magnetic moments of the spins but only in a tensorial sense (Figure 1*B*), leading to an interaction Hamiltonian, $\mathcal{H}_D = \gamma_I \gamma_S S \cdot \bar{\bar{D}} \cdot I$. Formally indistinguishable from this dipolar coupling but mediated by a different mechanism is the indirect $\bar{\bar{J}}$ interaction, which though essential in solution-state NMR, can usually be neglected in solid studies thanks to its small size. This is fortunate in view of the direct relation that then remains between the *I-S* coupling constant and the internuclear distance (r_{IS}^{-3}).

In addition to these magnetic effects, there is an important electric coupling that affects all nuclei with spin $S \geq 1$: the quadrupole interaction (Figure 1*C*) (11, 17). This arises from the classical energy E_Q between a nuclear charge distribution ρ and its surrounding electrostatic potential *V*:

$$E_Q = \int \rho(r) V(r) dr \approx \underset{\text{electrostatic energy}}{\text{point}} + \frac{1}{2} \sum_{i,j=x,y,z} \frac{\partial^2 V}{\partial i \partial j} \cdot \int ij\rho(r) dr \qquad 2.$$

$$+ \textit{higher-order terms} \ldots$$

Here $\frac{\partial^2 V}{\partial i \partial j} = V_{ij}$ denotes the electric field gradient at the nucleus, and its elements constitute an additional $3 \times 3\,\bar{\bar{V}}$ tensor; $Q_{ij} = \int ij\rho(r) dr$ is the classical

[1] A 3×3 tensor generalizes the concepts of scalar (an orientation-independent number) and vector (a 3-element array possessing a magnitude and a well-defined rotational transformation $V_i \rightarrow \sum R_{ij} V_j$) into one additional dimension. One way of building such Cartesian tensors is by arranging dyadic products between two vectors *V*, *U* into a 3×3 2-dimensional matrix: $A_{ij} = U_i V_j$.

description of the quadrupolar nuclear moment. E_Q is apparently unrelated to NMR, yet it can be shown that on deriving a quantum mechanical Hamiltonian $\mathcal{H}_Q$ for it, the elements Q_{ij} end up expressed in terms of spin operators.[2] The quadrupolar electrostatic energy terms in Equation 2 thus become the NMR-relevant spin Hamiltonian, $\mathcal{H}_Q = \frac{eQ}{4S(2S-1)} S \cdot \overline{\overline{V}} \cdot S$.

All these expressions for the nuclear spin Hamiltonians look similar: They involve products between a characteristic constant C_λ, a spin vector S, a coupling matrix, and another spin or B vector. Their generalized form is therefore

$$\mathcal{H}_\lambda = C_\lambda \overline{U} \cdot \overline{\overline{R}} \cdot \overline{V} = C_\lambda \sum_{i=1}^{3} U_i \sum_{j=1}^{3} R_{ij} V_j. \qquad 3.$$

The $\{R_{ij}\}_{i,j=1-3}$ matrices in these $\mathcal{H}_\lambda$ correspond to the shielding, dipolar or quadrupolar couplings ($\overline{\overline{\sigma}}$, D, V), interactions that depend on the chemical system under observation but not on the spin operators themselves.[3] Because physical rotations of the chemical system will change the individual R_{ij} values, these are collectively denoted as the *spatial* parts of the coupling Hamiltonian. The double sums in Equation 3, however, will end up generating other 3×3 tensors with matrix elements $\{T_{ij} = V_j U_i\}_{i,j=1-3}$ that do not involve any structural coupling parameters; they contain all of the $\mathcal{H}_\lambda$'s dependencies on the spin states, and are the quantum mechanical portions of the Hamiltonian operators. Thanks to this separation between spatial and spin terms, it becomes possible to express all local coupling Hamiltonians as $\mathcal{H}_\lambda = C_\lambda \overline{\overline{R}} \cdot \overline{\overline{T}}$, which is an extension of the scalar product between two vectors to the case of 3×3 tensors. This implies that when considering each individual interaction, its R and T components may change depending on the reference frame used for their description, but their resulting Hamiltonian will not: It is a scalar. Indeed, insensitivity to orientation is one of the most useful characteristics of zero-field magnetic resonance and pure quadrupole resonance, leading to sharp lines even when dealing with polycrystalline samples (1, 19).

There is actually more to the nature of the $\overline{\overline{R}}$ and $\overline{\overline{T}}$ tensors than just a 3×3 matrix character, particularly with regard to describing their changes upon rotating either the spatial or spin coordinates.[4] Indeed, as different reference frames are chosen all nine elements defining a tensor may change, yet certain key features are not really dependent on this choice and will remain constant. (For instance a

[2] A fundamental step in this derivation is the Wigner-Eckart theorem (18), stating that in systems with well-defined angular momentum the quantum mechanical expressions of all vector operators (e.g. x, y, z in Q_{ij}) are in fact proportional to one another (that is, to S_x, S_y, S_z).

[3] When external Zeeman or *rf* couplings are involved R_{ij} becomes δ_{ij}, the identity matrix.

[4] For the case of $\overline{\overline{R}}$ such rotations may be done for the convenience of expressing couplings in a new reference frame, or when accounting for a coherent mechanical motion like magic-angle spinning. $\overline{\overline{T}}$ rotations are usually used to describe the effects of *rf* pulses or nutations around magnetic fields rather than "physical" rotations, and correspond to stepping into alternative interaction representations.

shielding tensor $\bar{\bar{\sigma}}$ may vary upon rotating a molecule's frame, yet there is a certain isotropic chemical shift component, the one usually observed in solution phase experiments, that is invariant to reorientations.) This reflects the "reducibility" problem of Cartesian tensors, whose resolution requires rearranging the matrix elements into a series of objects that behave differently with respect to rotations. The resulting "irreducible" ranks make up mathematical groups, meaning that a rotation $\varepsilon(\alpha, \beta, \gamma)$ will not transform components $A_{ij}{}^{(k)}$ of rank k into elements $A_{ij}{}^{(k')}$ of a different rank k'. One such possible rearrangement, applicable to either the spin or spatial NMR tensors, is (18)

$$A^{(0)} = (A_{11} + A_{22} + A_{33})/3\text{: orientation-independent (scalar, zero-rank) component} \tag{4a}$$

$$A_{ij}^{(1)} = \frac{1}{2}(A_{ij} - A_{ji}) \quad i = 1\text{–}2,\ j = i + 1\text{–}3\text{: three first-rank components transforming as a vector} \tag{4b}$$

$$A_{ij}^{(2)} = \frac{1}{2}(A_{ij} + A_{ji}) - A^{(0)} i = 1\text{–}3,\ j = 1\text{–}3\text{: five second-rank components transforming as a } 3 \times 3 \text{ traceless symmetric matrix} \tag{4c}$$

Rather than using these definitions based on Cartesian coordinates, it is customary to take linear combinations within each rank to obtain a tensor's description in spherical coordinates, better behaved with respect to uniaxial rotations.[5] Even when written in this manner, the various elements of a particular tensor are represented as $\{A_{km}\}$, but k now refers to an element's rank and $m = -k, \ldots, k$ indicates its order. Such tensor elements transform under coordinate rotations according to

$$A_{km'} = \varepsilon(\alpha, \beta, \gamma) A_{km} \varepsilon^{-1}(\alpha, \beta, \gamma) = \sum_{m'=-k}^{+k} \mathcal{D}_{m'm}^{(k)}(\alpha, \beta, \gamma) A_{km'}, \tag{5.}$$

where the $\mathcal{D}_{m'm}^{(k)}$ define Wigner rotation matrix elements $e^{-im'\alpha} d_{m'm}^{(k)}(\beta) e^{-im\gamma}$ describing how elements within a rank k transform into one another (2, 20).

Truncation by B_o: First- and Second-Order Anisotropies

It follows from these arguments that the various internal NMR couplings can be expressed as products between irreducible spin and spatial spherical tensors possessing ranks $k \leq 2$. These products are orientation-independent scalars, but the dominating Zeeman coupling will break this symmetry and endow each spin interaction with an anisotropic character. This truncation imposed by $\mathcal{H}_Z$ on the

[5]This choice is not unlike the one taken for describing atomic orbitals, which can be expressed either as easily visualized Cartesian functions (e.g. p_x, p_y, p_z) or as better behaved spherical harmonics [$p_o = p_z$, $p+1 = -(p_x + ip_y)/\sqrt{2}$, $p_{-1} = (p_x - ip_y)/\sqrt{2}$]. It also reflects the fact that s orbitals transform as $A^{(0)}$, p as $A^{(1)}$, d as $A^{(2)}$, etc.

smaller $\mathcal{H}_\lambda$ can be appreciated in a number of ways: One is by using standard time-independent perturbation theory; another is by viewing the truncation as resulting from the fast time dependence that $\mathcal{H}_Z$ imposes on the smaller interactions. The latter derivation involves transforming the spin-space components of the $\mathcal{H}_\lambda$'s into an interaction representation, akin to the rotating frame usually employed in the classical description of NMR (1, 9, 11). This is defined quantum mechanically by the time propagator $U_o(t) = exp(-i\mathcal{H}_Z t) = exp(i\omega_o S_z t)$, representing a continuous rotation at a rate ω_o around S_z, the spin-space's z-axis. Thanks to the well-behaved nature of the spherical tensor operators with respect to z-rotations ($e^{iS_z\phi}T_{km}e^{-iS_z\phi} = T_{km}e^{-im\phi}$), this can be simply accounted for as

$$\tilde{\mathcal{H}}_\lambda(t) = U_0(t)^{-1}\mathcal{H}_\lambda U_0(t) = C_\lambda \sum_{k=0}^{2}\sum_{m=-k}^{k} R_{k-m}T_{km}e^{-im\omega_0 t}. \qquad 6.$$

At first sight this transformation seems to have worsened matters by making the $\mathcal{H}_\lambda$ time dependent, but this complication can be dealt with using a versatile approximation known as average Hamiltonian theory (AHT) (2, 21). According to AHT, the effective evolution introduced on all $\tilde{\mathcal{H}}_\lambda$'s at the end of each periodic Larmor cycle $\tau_c = 2\pi/\omega_o$ can be approximated as the time-independent series

$$\overline{\mathcal{H}_{\text{total}}}(\tau_c) = \sum_{\lambda\neq Z}\mathcal{H}_\lambda^{(1)} + \sum_{\lambda,\lambda'\neq Z}\mathcal{H}_{\lambda,\lambda'}^{(2)} + \cdots, \qquad 7.$$

where the leading terms are

$$\mathcal{H}_\lambda^{(1)} = \tau_c^{-1}\int_0^{\tau_c}\tilde{\mathcal{H}}_\lambda(t)dt, \quad \mathcal{H}_{\lambda,\lambda'}^{(2)} = \frac{-i}{2}\tau_c^{-1}\int_0^{\tau_c}dt\int_0^{t}[\tilde{\mathcal{H}}_\lambda(t), \tilde{\mathcal{H}}_{\lambda'}(t')]dt'. \qquad 8.$$

It follows from Equation 6 that the first of these terms will only preserve the time-independent $m = 0$ elements. For the shielding, dipolar, and quadrupolar interactions this leads to the dominant first-order Hamiltonians (2–6)

$$\mathcal{H}_{CS}^{(1)} = -\gamma\left(R_{00}^{CS}T_{00}^{S} + R_{20}^{CS}T_{20}^{S}\right) = -\gamma B_0\left(R_{00}^{CS} + R_{20}^{CS}\right)S_z = \left(\omega_{CS}^{iso} + \omega_{CS}^{aniso}\right)S_z \qquad 9a.$$

$$\mathcal{H}_D^{(1)} = \gamma_I\gamma_S R_{20}^{D}\cdot\begin{cases} T_{20}^{IS} = \omega_D(3I_zS_z - I\cdot S)/2 & \text{if } \omega_0^I = \omega_0^S \\ T_{10}^{I}T_{10}^{S} = \omega_D I_zS_z & \text{if } \omega_0^I \neq \omega_0^S \end{cases} \qquad 9b.$$

$$\mathcal{H}_Q^{(1)} = \frac{eQ}{4S(2S-1)}\cdot R_{20}^{Q}T_{20}^{S} = \omega_Q[3S_z^2 - S(S+1)]. \qquad 9c.$$

Thus, the only isotropic term arising from these couplings comes from the chemical shift ω_{CS}^{iso}, with all remaining ones leading to spatial anisotropies that transform as second-rank R_{20}^{λ} tensors.

In most cases these first-order Hamiltonians, proportional to coupling constants C_λ, are excellent descriptions of H_λ's complete effects. The following terms in the expansion are proportional to $C_\lambda C_{\lambda'}/\omega_0$ and therefore inconsequential, except when dealing with $S \geq 1$ nuclei subject to large quadrupole effects. Indeed,

quadrupole coupling constants can often lie in the MHz range (17, 22), and thereby lead to cross terms $\mathcal{H}^{(2)}_{\lambda,Q}$ that are easily detectable by NMR. Most notable among these is the second-order quadrupole effect

$$\mathcal{H}^{(2)}_{Q,Q} = \frac{C_Q^2}{\omega_0} \sum_{m\neq 0} \frac{R_{2m} R_{2-m}[T_{2m}, T_{2-m}]}{2m}, \qquad 10.$$

which like all remaining second-order correlations, brings out new products of both spatial ($R_{2m}R_{2-m}$) and spin ($T_{2m}T_{2-m}$) spherical tensor components.[6] In the same manner that dyadic multiplications of rank-1 vectors lead to second-rank tensors, such products of rank-2 terms will lead to tensors with $k \leq 4$ (23, 24). Symmetry considerations force the order of all elements in this multirank expansion to $m = 0$; further calculations indicate that the products of the spatial tensor components will result in a zero-rank (R^Q_{00}) term analogous to ω^{iso}_{CS} but of quadrupole origin, as well as to second-rank (R^Q_{20}) and fourth-rank (R^Q_{40}) anisotropies. Higher-rank spin-space components will also arise, with the commutators in Equation 10 leading only to odd (T_{10}, T_{30}) terms. When dealing with the central $-\frac{1}{2} \leftrightarrow +\frac{1}{2}$ transition of a half-integer quadrupolar spin ($S = \frac{3}{2}, \frac{5}{2}, \ldots$), which is the only single-quantum transition in these systems that is not affected by the otherwise dominating $\mathcal{H}^{(1)}_Q$ term, both of these operators are proportional to the longitudinal central-transition angular momentum C_z. Therefore, from a spin-space perspective, the type of precession that $\mathcal{H}^{(2)}_{Q,Q}$ imparts on the central transition of these nuclei is akin to that of a chemical shift.

Spin Evolution and the Calculation of NMR Spectra

To calculate the spins' NMR signal after they have been taken away from equilibrium, it is convenient to represent their ensemble by a density matrix ρ that accounts for both the quantum-mechanical nature of the spins and their incoherent statistical superposition (1–13). The spin evolution can then be obtained from integrating Schröedinger's equation as

$$\rho(t) = U(t)\rho_o U(t)^{-1}; \quad U(t) = \exp\left[-i\int_0^t \mathcal{H}(t')dt'\right], \qquad 11.$$

where the operator $U(t)$ describes the dynamics imposed by a rotating frame Hamiltonian like the one in Equation 7 on spins assumed in an initial state ρ_o. The small voltage induced by the spins along a transverse coil can then be derived as $S(t) = Tr[\rho(t)S_+]$.

The density matrix ρ is itself an operator, and can thus be expressed as a linear combination of various spin-space terms (S_z, S_x, T^S_{20}, etc). For instance, an initial

[6] Additional terms $R_{2m}R_{20}[T_{2m}, T_{20}]$ representing a tilting in the axis of quantization survive the double time integration in Equation 8, but can be neglected to this degree of approximation.

thermal equilibrium state dictated by the Zeeman interaction will be

$$\rho_{eq} = e^{-\mathcal{H}_z/kT} \approx 1 + \frac{\omega_0}{kT} S_z \sim \frac{\omega_0}{kT} S_z, \qquad 12.$$

where the "1" represents unpolarized spins that remain indifferent to all NMR manipulations and thereby can be ignored. Such an operator description thus results in a state that is analogous to the *z*-magnetization that could be expected from a classical perspective. Furthermore, the action of single-spin $\mathcal{H}_{rf} = \omega_{rf} S_x$ or $\mathcal{H}_{CS} = \omega_{CS} S_z$ Hamiltonians can be rigorously described according to

$$\begin{aligned} S_z &\xrightarrow{\omega_{rf} S_x t} S_z \cos(\omega_{rf} t) - S_y \sin(\omega_{rf} t); \\ S_x &\xrightarrow{\omega_{CS} S_z t} S_x \cos(\omega_{CS} t) + S_y \sin(\omega_{CS} t), \end{aligned} \qquad 13.$$

where the left-hand operators denote prototypical ρ_o states, the arrows are shorthand for the evolution operators, and the right-hand sides show the $\rho(t)$. Again there is a one-to-one correspondence between these equations and the expectations that result from classical predictions. This parallelism is maintained for as long as linear single-spin interactions are involved[7] but ceases to be complete in more complex cases containing either quadrupolar or spin-spin couplings, for which states not describable by single-spin operators appear. In an effort to preserve even for these cases the simplicity of the spin-½ notation a formalism was developed, in which the new states are described as direct multiplications of single-spin operators. Hence, the effects of heteronuclear dipolar or $S = 1$ quadrupolar couplings can be described as (9, 10)

$$\begin{aligned} S_x &\xrightarrow{\omega_D I_z S_z t} S_x \cos\frac{\omega_D t}{2} + 2 S_y I_z \sin\frac{\omega_D t}{2}; \\ S_x &\xrightarrow{\omega_Q \left[3S_z^2 - S(S+1)\right] t} S_x \cos\omega_Q t + 2(S_y S_z + S_z S_y)\sin\omega_Q t. \end{aligned} \qquad 14.$$

The contributions made by these spin-product states to the NMR signal is easy to visualize: Functions that are multiplying single-quantum, in-phase operators (S_x, S_y) are directly detectable by the NMR coil; single-quantum antiphase coherences containing only one transverse operator ($I_z S_y$, $S_z S_y$) are not directly observable but can lead to in-phase signals if acted upon by suitable couplings; spin-order or multiple-quantum states possessing only longitudinal or several transverse operators are not observable unless acted upon by further pulses.

This elegant formalism is particularly suitable for describing experiments defined by commuting interactions, such as chemical shifts and/or weak spin-spin couplings. Such conditions are widespread in solution but not always met in solid state NMR; here interactions may be time-dependent and not mutually commuting, and couplings comparable if not larger than the *rf* fields. Analytical descriptions

[7]This "coincidence" actually reflects a local isomorphism between the elements of the SO(3) space group defining vector rotations in an orthogonal three-dimensional space, and the SU(2) group defining unitary transformations $U(t)$ for 2×2 matrix operators such as those describing isolated spin-1/2 ensembles.

of the spins' evolution may then be difficult to come by, and alternatives are needed for evaluating the experimental results. A common approximation is AHT (Equation 7), which can provide a hierarchical expansion of the effects introduced by periodically time-dependent interactions if the system is probed at proper integer multiples of the modulation period (25). A conceptual and practical alternative for dealing with periodic manipulations is Floquet theory (26, 27), which bypasses the problems associated with finding the evolution imposed by a time-dependent interaction by deriving an alternative Hamiltonian that is time-independent but possesses an infinite dimension.[8] Finally, a general route to the calculation of arbitrary spin evolutions consists of propagating density matrices throughout an interval of interest t by subdividing the time axis into short enough periods Δt. Computations of the evolution operator can then proceed on the assumption of piecewise constant Hamiltonians as $U(0,t) \approx \ldots e^{-i\mathcal{H}(\Delta t)\Delta t} e^{-i\mathcal{H}(0)\Delta t}$. Such a procedure can be highly time consuming, particularly when dealing with powdered samples containing multiply coupled or high-spin nuclei and subject to arbitrary time dependencies; alternatively, certain simplifying assumptions (tensor symmetries, stroboscopic observation) can be exploited, and numerous useful algorithms have been proposed for facilitating solid state spectral simulations under a variety of conditions (28–32).

HIGH RESOLUTION IN SOLIDS NMR

Averaging via Spin-Space Manipulations

Given the different information conveyed by the spin interactions and the orientation-dependence brought upon them by the high field Zeeman truncation, the selective removal of couplings and/or of their anisotropic components becomes an important topic in solid state NMR. The complete elimination of anisotropies becomes particularly relevant when dealing with randomly powdered samples and trying to resolve the broadened signals arising from chemically inequivalent sites. Because NMR Hamiltonians are given by products of spin (T^{λ}_{k0}) and spatial (R^{λ}_{k0}) terms, such selective eliminations can generally involve imposing a time dependence on the spin components of $\mathcal{H}_{\lambda}$ via *rf* irradiations, on their spatial components via mechanical sample reorientations, or sometimes on both spin and spatial components.

Perhaps the simplest relevant example of selective spin-space averaging is heteronuclear decoupling, which removes the effects of $\mathcal{H}^{IS}_{D}$ from an S spectrum by continuously irradiating I close to resonance (2). The application of such an *rf* field can be accounted for by an evolution operator $U_{rf}(t) = exp[i\omega_{rf} I_x t]$, which

[8]The resulting Floquet Hamiltonian is no longer defined on the conventional spin manifold $\{|\alpha\rangle, |\beta\rangle\}$ but on a "dressed" basis set $\{|\alpha m\rangle, |\beta m\rangle\}$ associated with a spin state as well as with a multiple mode of the basic modulating frequency; practical calculations involve diagonalizing this Hamiltonian after it has been truncated to a sufficiently high order and then exploiting it to compute the spins' evolution at arbitrary times.

leaves S unaffected but imparts on the I-containing terms in the Hamiltonian a time-modulation

$$\mathcal{H}_D^{IS} + \mathcal{H}_{CS}^{I} \xrightarrow{U_{rf}} \tilde{\mathcal{H}}(t) = \omega_D S_z (I_z \cos \omega_{rf} t - I_y \sin \omega_{rf} t) - \Delta\omega_I (I_z \cos \omega_{rf} t - I_y \sin \omega_{rf} t), \quad 15.$$

where $\Delta\omega_I$ is the *rf* irradiation offset. This time evolution is akin to the one expected from classical nutation arguments, and it clearly makes $\mathcal{H}_D = 0$, at least to first-order in AHT and when $\Delta\omega_I = 0$. Continuous irradiation is consequently a method of choice for achieving heteronuclear (e.g. $\{^1H\}^{13}C$) decoupling in the solid state (14, 33, 34). When the rates of nutation ω_{rf} are not fast enough, however, second-order terms $\mathcal{H}_{CS,D}^{(2)} \propto (\Delta\omega_I \cdot \omega_D/\omega_{rf}) S_z I_x$ arising from offset/dipolar cross correlations may become relevant (35). These residuals are generally present in the case of ^1H-decoupling in organic solids due to site inequivalencies and/or shielding anisotropies (36); they are not susceptible to complete elimination by concurrent sample spinning, and are consequently important factors in broadening the S-spin resonances.[9] In such cases it is possible to improve the decoupling performance by imposing a second time dependence on the spins that, acting orthogonally to I_x, helps quench the $\mathcal{H}_{CS,D}^{(2)}$ residual (37, 38). This is most often implemented with a simple "two-pulse phase modulated" (TPPM) scheme, although more sophisticated alternatives have also been described (39, 40).

An equivalent way of visualizing heteronuclear decoupling is by considering the rotations induced by $U_{rf}(t)$ on the first-rank spin-space elements (Equation 5):

$$T_{10}^{I} \xrightarrow{U_{rf}} \tilde{T}_{10}^{I}(t) = d_{00}^{(1)}(\beta) T_{10}^{I} + d_{10}^{(1)}(\beta) T_{11}^{I} e^{-i\omega_{rf}t} + d_{-10}^{(1)}(\beta) T_{1-1}^{I} e^{i\omega_{rf}t}; \quad 16.$$

fast oscillations will then average out the $\left\{T_{1\pm1}^{I}\right\}$, whereas the choice of transverse *rf* ($\beta = 90^\circ$) eliminates the first-order spherical harmonic $d_{00}^{(1)}(\beta) = \cos\beta$. By contrast, spin terms in the homonuclear $\mathcal{H}_D^{IS} = \omega_D R_{20}^{IS} T_{20}^{IS}$ couplings transform as second-rank tensors and therefore will fail to average out under these conditions. Instead, removing second-rank components requires fast nutations around an axis inclined at the root of $d_{00}^{(2)}(\beta) = (3\cos^2\beta - 1)/2$, the magic angle $\beta_m = 54.7^\circ$. A continuous version of this averaging is achieved in the Lee-Goldburg (LG) experiment (41), which applies an *rf* field that is offset from resonance by $\Delta\omega_{LG} = 0.71\omega_{rf}$ (Figure 2). The ensuing spin-space rotation does not occur at a root of T_{10}; first-rank tensors such as the chemical shift will then be scaled but not eliminated, thereby enabling the acquisition of shift-based NMR spectra from strongly coupled networks such as protons in organic solids.

Although important as a conceptual starting point, LG experiments are rarely employed in high-resolution acquisitions owing to a number of limitations, including a lack of observation windows, difficulties in strictly fulfilling the first-order

[9]Residual couplings also arise when magic-angle spinning (MAS) rates or small integer multiples thereof approach the rates of nutation ω_{rf}, as manifestations of rotary resonance recoupling (see "Chemical Shift/Heteronuclear Coupling Correlations" below).

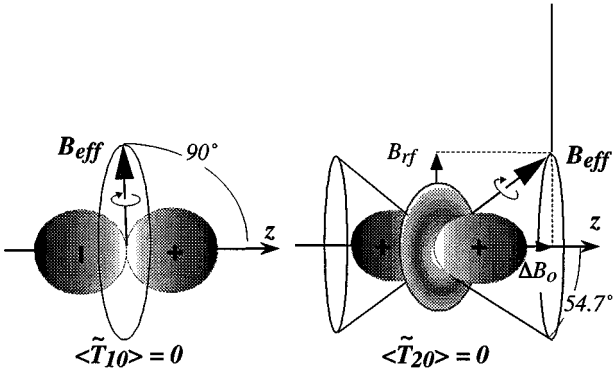

Figure 2 Averaging of first (T_{10})– and second (T_{20})–rank spin-space tensors by continuous rotations around effective fields inclined at $d^{(\ell)}_{00}(\beta_m) = 0$. Prior to irradiation only the z-direction of spin-space is defined (by B_o); hence the axial symmetry.

averaging regime, and high sensitivity to inhomogeneities in ω_{rf}. Multiple-pulse sequences in which the continuous T^{IS}_{20} rotation introduced by LG irradiation is replaced with compensated reorientations separated by windows of free evolution can alleviate all these limitations (21). As in the continuous LG version, the "toggling" motion imposed by these discrete spin-space manipulations on the interaction-frame Hamiltonians needs to fulfill an effective tetrahedral symmetry. This will then average out second- (but not necessarily first-) rank couplings, while overcoming nonidealities stemming from pulse imperfections and higher-order ($\mathcal{H}^{(2)}_{D,CS}, \mathcal{H}^{(2)}_{D,rf}$) interferences. Over the years numerous principles have been developed to meet these ends, and many of them serve as useful general guidelines in the development of solid- and liquid-state pulse sequences (2, 5, 6). One such principle relates to the fact that all even-numbered imperfections in the AHT series may be eliminated by "symmetrizing" the interaction Hamiltonian over the decoupling cycle (42); this in turn entails concatenating into a single "supercycle" period $2\tau_c$ two interaction Hamiltonians fulfilling $\{\tilde{\mathcal{H}}(t)\}_{0\le t\le\tau_c} = \{\tilde{\mathcal{H}}(\tau_c - t)\}_{\tau_c\le t\le 2\tau_c}$.[10] Another compensating principle relies on the fact that regardless of the complexity that may characterize higher-order multipulse imperfections, the spin parts of their effective Hamiltonians can still be written as linear combinations of T_{km}'s (44). Given the well-defined rotational properties exhibited by these residual terms with respect to z-axis rotations, repeating the complete decoupling cycle with all pulses shifted by phase $\Delta\phi_j = 2\pi j/N$ will impose phase shifts $T_{km}e^{-im\Delta\phi_j}$ on these imperfections and eventually remove

[10] In the LG case τ_c corresponds to $(\omega^2_{rf} + \Delta\omega^2_{LG})^{-1/2}$, and the time reversal can be carried out by simultaneous frequency shifts $\Delta\omega_{LG} \leftrightarrow -\Delta\omega_{LG}$ in coordination with 180° phase inversions of the *rf*. This is the principle of the much more efficient "frequency-shifted LG" (FSLG) experiment (43).

them when summed over a sufficiently large number of cycles N.[11] All these guidelines need to be exercised with care lest they eliminate the desired chemical shift observables together with the imperfections, or end up lasting too long for their AHT premises to remain valid; still, it has been shown that the gains resulting from following them amply overcome their drawbacks.

Averaging First-Order Couplings via Spatial Space Manipulations

Whereas spin-space components vary from coupling to coupling, all first-order spatial anisotropies transform as spherical harmonics of rank-2. In analogy with the LG experiment these can be modulated by imposing on the R^{λ}_{20} the time dependence that arises upon rotating the sample—now mechanically, in real coordinate space. Spinning at an angle β with respect to B_o then results in

$$R^{\lambda}_{20} \xrightarrow{\text{spinning}} \tilde{R}^{\lambda}_{20}(t) = \sum_{m=-2}^{2} d^{(2)}_{m0}(\beta) e^{-im\omega_r t} R^{\lambda}_{2m}(\Omega), \qquad 17.$$

where Ω is a set of angles transforming the spatial coupling tensor into a reference frame fixed on the spinning rotor. $\tilde{R}^{\lambda}_{20}(t)$ thus includes four terms oscillating at frequencies $\pm\omega_r$, $\pm 2\omega_r$ (also expressible as cosines and sines of $\omega_r t$, $2\omega_r t$), plus a constant term proportional to $d^{(2)}_{00}(\beta)$. In the $\omega_r \gg \omega_\lambda$ fast-spinning regime the $\pm m\omega_r$ oscillations occur so rapidly that the $\{R^{\lambda}_{2m}\}_{m\neq 0}$ terms cannot impose a substantial net evolution; the residual is then a constant $R^{\lambda}_{20}(\Omega)$ identical in form to the static interaction, except for the $d^{(2)}_{00}(\beta)$ scaling. As a function of spinning angle $0^\circ \leq \beta \leq 90^\circ$ this scaling factor sweeps monotonically the $[1, -0.5]$ interval, and for the sake of high resolution its key value is $\beta_m = 54.7^\circ$ magic angle spinning (MAS), for which $d^{(2)}_{00}(\beta_m) = 0$ (45, 46).

Equation 17 entirely describes the modulation imposed by sample spinning on the spatial components of the $\mathcal{H}_\lambda$ interactions, but the actual fate of the spin coherences will depend as well on the type of interaction being averaged (13, 23). Most important is whether the various spin parts of the $\mathcal{H}_\lambda$'s rendered time dependent by the sample rotation commute with one another or not. They do, for instance, when considering shielding, heteronuclear dipolar, or first-order quadrupolar interactions. In these cases the time evolution can be accurately described as

$$U(t) = T \exp\left[-i \int_0^t \mathcal{H}_\lambda(t')dt' \right] = e^{-i\omega_\lambda(t)S_z}, \qquad 18.$$

[11] This is an example of second averaging, in which residuals of a partly averaged interaction are further reduced by imposing an additional (slower) time dependence. Decoupling itself, for example, can be viewed as second averaging of the secular residuals left by the B_o truncation.

and then the spins' evolution is as in Equations 13 and 14 except for the fact that couplings ω_λ are no longer constant but have time- and orientation-dependent expressions.[12] The free precession of spins under MAS can then be represented by an ensemble of magnetizations, each one associated with a different single crystallite in the sample and possessing an evolution phase (23, 47)

$$\phi(t) = \omega_{CS}^{iso} t + \sum_{\lambda} \sum_{m=-2}^{2} \omega_{2m}^{\lambda}(\Omega)\left[e^{im\omega_r t} - 1\right]/m\omega_r. \qquad 19.$$

All such "spin packets" in a powder thus begin their evolution in the perfect state of alignment that follows excitation but dephase throughout a rotor period as they become affected by different anisotropic evolution frequencies $\omega_{2m}^{\lambda}(\Omega)$. At the end of each period T_R, however, when $e^{im\omega_r T_R} = 1$, the cumulative effects of these anisotropic evolutions vanish regardless of crystallite orientation, and all packets meet again at a phase dictated solely by the isotropic shift (Figure 3*A*). Because of the intervening dephasing between 0 and T_R, MAS signals from inhomogeneously broadened systems such as these usually adopt the form of rotational echo trains, whose spacing and extent of dephasing scales as ${\omega_r}^{-1}$ (Figure 3*B*). This is reflected in the frequency-domain spectra as sets of sharp spinning sidebands flanking the isotropic centerbands at multiples of $N\omega_r$ [where $N \approx O(\omega_\lambda/\omega_r)$], which can convey valuable information on the anisotropic coupling parameters (48). This unassisted MAS technology finds its widest use in the averaging of dilute spin-½ shielding anisotropies (^{13}C, ^{15}N, ^{31}P) and in the line-narrowing of moderate first-order quadrupole broadening (^{2}H) (4, 34). For moderately symmetric environments and at relatively high fields MAS can also yield considerably sharp ^{14}N resonances and enable the resolution of chemically inequivalent nitrogen sites, though this requires an inordinately high accuracy ($\leq 0.01^\circ$) in the setting of β_m (49, 50).

Different considerations may arise when MAS is used for averaging out couplings that include the homonuclear dipole interaction (6, 23, 51). Actually, a pure $\mathcal{H}_D^{IS}(t) = T_{20}^{IS} \cdot \tilde{R}_{20}^{IS}(t)$ two-spin interaction is analogous to a first-order quadrupole coupling, and as in the latter case spectra will break up into sharp MAS sideband manifolds even when $\omega_r \ll \omega_D$. Isolated pairs of equivalent spins, however, are hardly typical when considering systems such as protons in organic solids, and realistic analyses need to account for the presence of multiple (*I-S*, *I-J*, ...) dipole couplings as well as for isotropic and anisotropic shieldings. The spin-space components of these various interactions do not commute among themselves, thereby rendering the overall coupling homogeneous and quenching MAS's averaging effects unless fast ($\gg\omega_D$) spinning rates are employed. Further insight into the effects of sample spinning can be gathered from an AHT expansion of the time-dependent MAS Hamiltonian in powers of ω_r^{-1}, which yields an $\mathcal{H}_D^{(1)}$ that is identically zero and centerband residuals that at high speeds will be dominated

[12]This self-commutation corresponds to cases of inhomogeneous broadenings, which in time-independent systems can be distinguished by their susceptibility to spectral hole burning.

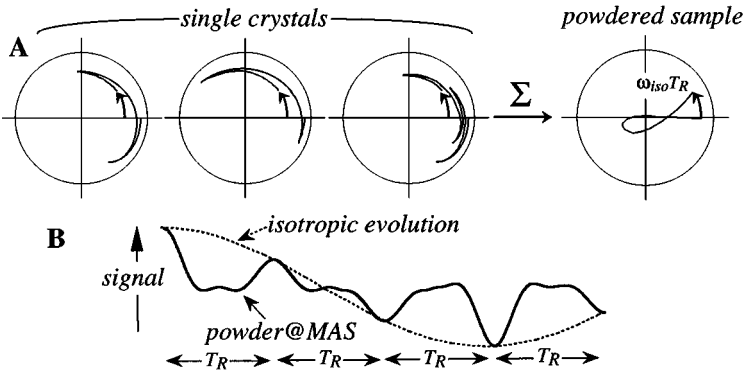

Figure 3 (*A*) *x-y* trajectories executed throughout the course of a rotor period by magnetization vectors subject to mutually self-commuting interactions [single-crystal trajectories were progressively contracted for presentation purposes (47)]. (*B*) Comparison of the powder MAS signals expected in these cases and their purely isotropic counterpart for multiple rotor periods.

by $\mathcal{H}^{(2)}_{D,D} \propto [\mathcal{H}^{IS}_D, \mathcal{H}^{IJ}_D]/\omega_r$ terms. As spinning rates increase, a progressive $\omega_r^{-\alpha}(\alpha = 1\text{–}1.5)$ scaling is indeed observed experimentally (51, 52), yet this is a fairly shallow ω_r dependence, which suggests that unassisted MAS will only become competitive vis-a-vis multiple pulse at very high (≈50–100 kHz) spinning rates (53). There are, however, a number of aids that can endow unassisted MAS with a positive role in the high-resolution solid state NMR of abundant nuclei. One is isotopic dilution, which in combination with currently attainable spinning rates yields narrow ^{1}H lines even at modest levels (54); another may be increasing the magnetic field strength, and spreading the chemical shifts of inequivalent coupled sites until the homogeneous character of their couplings is alleviated.[13]

Manipulating Second-Order Quadrupolar Interactions

As alluded to earlier, second-order effects become particularly relevant when focusing on the central $-1/2 \leftrightarrow +1/2$ transitions of half-integer quadrupolar nuclei, unaffected to first-order by quadrupolar couplings thanks to their S_z^2 dependence (Equation 9c) (17, 22). On attempting to remove the residual anisotropic components of these second-order $\mathcal{H}^{(2)}_{Q,Q}$ interactions via spatial manipulations, one is confronted with a factor $d^{(2)}_{00}(\beta)$ that will scale the second-rank broadening R^Q_{20}, as well as with a factor $d^{(4)}_{00}(\beta) = (35\cos^4\beta - 30\cos^2\beta + 3)/8$ that will scale R^Q_{40}. Either of these polynomials can be set to zero at certain spinning angles, yet their roots are not coincident, and therefore no single "magic" axis of rotation will

[13] Such a regime has already materialized for the case of ^{19}F NMR, which though abundant, possesses a much wider chemical shift scale than ^{1}H and for which available MAS rates (25–50 kHz) can provide good spectral resolution (55).

simultaneously remove all their associated second-order broadenings. This single-axis spinning deficiency can be overcome by introducing more complex forms of mechanical reorientation: multiple-axes spinning strategies (24, 56, 57). Among these, perhaps conceptually closest to MAS is double-rotation (DOR), in which the quadrupole-containing powdered sample is simultaneously spun around two axes, β_1 and β_2 (58). An extension of the formalism described earlier for MAS (Equation 17) reveals that nonoscillating k-rank anisotropies will be scaled in this case by $d_{00}^{(k)}(\beta_1)d_{00}^{(k)}(\beta_2)$, and therefore all broadenings can be removed if the noncoincident spinning axes are set at the magic angles of the second- and fourth-rank spherical harmonics. An alternative that narrows the central transitions in a technically easier manner consists of consecutively spinning the sample around two different β_1, β_2 axes, each associated with their own evolution times t_1, t_2 (59). The choice of spinning angles in such dynamic-angle-spinning (DAS) experiments is more flexible than in DOR, as all that is demanded is the pointwise cancellation of anisotropies according to

$$d_{00}^{(2)}(\beta_1)t_1 = -d_{00}^{(2)}(\beta_2)t_2; \quad d_{00}^{(4)}(\beta_1)t_1 = -d_{00}^{(4)}(\beta_2)t_2. \qquad 20.$$

At the conclusion of these evolution times a purely isotropic echo forms, and by synchronously increasing the duration of (t_1, t_2) a high resolution signal becomes available. The stepwise nature of this refocusing implies that anisotropies are not instantly removed as in other averaging methods discussed so far but appear, after a two-dimensional (2D) Fourier transformation of $S(t_1, t_2)$, correlated along a sharp ridge for every single-crystallite in the sample. Therefore, unlike MAS, DAS does not bring with its higher resolution an effective increase in signal-to-noise; in fact, signal is lost by virtue of the need for "storing" the evolving coherences along B_o while the spinning axis is reoriented from β_1 to β_2.[14]

A refocusing similar to that carried out by DAS but involving a single axis of sample rotation is feasible if the restriction to central transition observations is lifted (61, 62). Indeed, it follows from the spin energy diagram for half-integer quadrupole nuclei (Figure 4) that not only the central but in fact any $-m \leftrightarrow +m$ multiple-quantum (MQ) transition will be free from the dominant first-order quadrupole broadenings. Yet second-order effects will still influence these transitions. This opens up the possibility of compensating the residual $\mathcal{H}_{Q,Q}^{(2)}$ broadenings affecting the $-\frac{1}{2} \leftrightarrow +\frac{1}{2}$ evolution, with the $\mathcal{H}_{Q,Q}^{(2)}$ anisotropies affecting other symmetric MQ transitions. To evaluate such a possibility it is pertinent to include the transition order m in the description of the second-order frequencies, whose

[14] "Storage" is a widespread way of protecting the phase encoded by evolving magnetizations while a relatively slow process like a sample hop is taking place. It involves rotating (with a pulse) spin coherences away from the x-y plane and into the B_o axis, where they can reside for times in the order of T_1 without evolving or losing their original encoding (4, 60). Owing to their low symmetry, storage pulses can only conserve an axial projection of the transverse x-y magnetization, thus decreasing the signal observed upon recall by an average factor of two (plus losses to T_1 relaxation and/or spin diffusion).

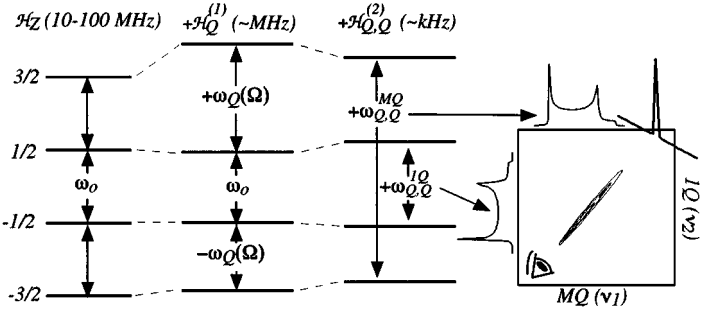

Figure 4 Hierarchical description of Zeeman plus quadrupolar effects on an $S = 3/2$ energy diagram, illustrating how all anisotropies can be removed by correlating under MAS multiple-quantum and central single-quantum transitions within a 2D NMR experiment.

average under rapid sample spinning becomes

$$\omega_{Q,Q}^{-m\leftrightarrow+m}(m,\beta) = C_S^{(0)}(m)\omega_Q^{(0)} + C_S^{(2)}(m)d_{00}^{(2)}(\beta)\omega_Q^{(2)}(\Omega) + C_S^{(4)}(m)d_{00}^{(4)}(\beta)\omega_Q^{(4)}(\Omega), \quad 21.$$

where the $\{\omega_Q^{(k)}\}_{k=0-4}$ denote the zero-, second-, and fourth-rank frequency contributions, and the $\{C_S^{(k)}(m)\}_{k=0-4}$ are polynomials that depend on the spin S and transition order m involved. According to this expression, m imparts on the spin evolution, via the $C_S^{(k)}$-polynomials, an effect similar to that played by β through the $\{d_{00}^{(k)}\}$. Therefore, two analogous routes open up for averaging out second-order $\omega_{Q,Q}$ anisotropies: to keep $m = 1/2$ constant and make β time dependent (DAS), or to keep β constant at MAS while making m time dependent through MQ $\leftrightarrow$ 1Q 2D correlations. Experimentally, the latter is a simpler route, whereas from a practical standpoint it has the advantage of concurrently averaging out all remaining shielding and dipolar anisotropies. An important issue in these 2D MQMAS experiments is the optimized manipulation of the MQ excitation and conversion processes; intensive research in this area is being performed (63–72), and sequences that in favorable cases achieve a DAS-like sensitivity have been developed. Also promising is the recent realization that 2D MAS correlations between central and satellite transitions can achieve a similar type of refocusing, even though they involve only single-quantum correlations (73).

CROSS POLARIZATION

Cross Polarization Transfers Between Spin-1/2

Collecting solid NMR spectra can be particularly challenging for dilute low-γ nuclei with inherently low sensitivities and long relaxation times (e.g. ^{13}C, ^{15}N, ^{17}O, ^{25}Mg, ^{67}Zn). Throughout the years one technique has proven instrumental for bypassing this signal to noise (S/N) limitation: double-resonance cross polarization (CP) (33, 74). New perspectives have emerged on the effects that fast MAS and

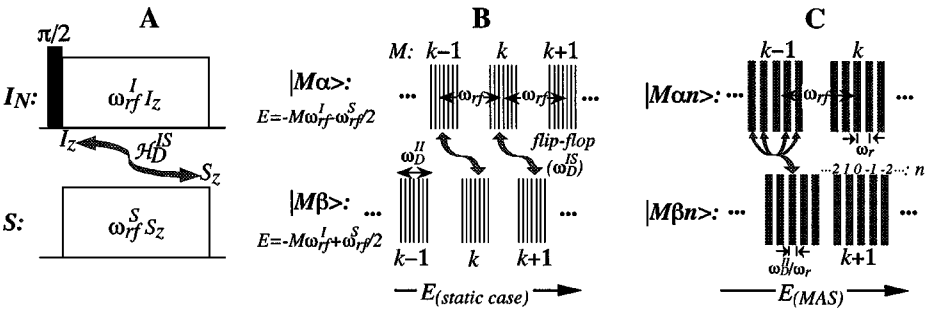

Figure 5 (*A*) Cross polarization pulse sequence and *rf* operators in the doubly-tilted rotating frame. (*B,C*) Ensuing energy-level diagrams for static and fast magic-angle spinning cases. An efficient cross polarization requires the ω_D^{IS}-driven flip-flop effect to be secular, i.e. to have its interconnected energy levels matched up.

quadrupole couplings may have on this sequence, which are worth bringing up in this discussion.

CP transfers polarization from an abundant *I*- (usually ^{1}H) to a rare *S*-spin reservoir, thereby increasing the latter's signal by $\sim\gamma_I/\gamma_S$ while making the repetition time of the experiment dependent on the usually much shorter T_1^I time. Two conditions make this $I \rightarrow S$ transfer possible: the generation of a perturbed *I* state seeking a return to equilibrium via the discharge of its excess polarization, and the establishment of an *I-S* coupling Hamiltonian that enables this excess to relax primarily into observable *S* magnetization. In pulsed CP (Figure 5*A*) the first of these conditions is achieved via spin-locking, a $\pi/2$ pulse followed by a rapid phase shift that places the B_o-equilibriated *I* magnetization into the *x-y* plane and parallel to a transverse *rf* field $B_{rf}^I \ll B_o$. Such an *rf* field would normally result in the decoupling of *I* and *S* reservoirs, but during CP this is prevented by the simultaneous application of a B_{rf}^S field tuned at the same nutation frequency, $\omega_{rf}^S = \omega_{rf}^I$. This imparts on neighboring *I*- and *S*-nuclei identical longitudinal oscillation frequencies, making them look, in a suitable interaction frame, like a homonuclear spin pair capable of undergoing back-and-forth transfers of magnetization. Reaching this frame requires a 90° tilt of the *I*, *S* quantization directions that places both *rf* fields along redefined *z*-axes, followed by a rotating-frame transformation $\exp[-i(\omega_{rf}^I I_z + \omega_{rf}^S S_z)t]$ which truncates chemical shifts, scales homonuclear *I-I* couplings by $-\frac{1}{2}$, and leaves a heteronuclear dipole Hamiltonian $\mathcal{H}_D^{IS} = \omega_D(I_x S_x + I_y S_y)$ containing a flip-flop exchange character. An *I*-spin state initially prepared parallel to B_{rf}^I will then transform as (13)

$$\rho_0 = \gamma_I I_z \xrightarrow[\mathcal{H}_D^{IS}]{\omega_{rf}^I = \omega_{rf}^S} \gamma_I \left[I_z \left(\frac{1+\cos\omega_D t}{2} \right) + S_z \left(\frac{1-\cos\omega_D t}{2} \right) + (I_x S_y - I_y S_x)\sin\omega_D t \right]. \qquad 22.$$

These transfer functions evidence that an S_z polarization will grow along B^S_{rf} in an oscillatory fashion that is closely related to the cos ($\omega_D t$) dipolar signal, and potentially result in a net γ_I/γ_S enhancement. The fine structure of this $I_z \rightarrow S_z$ transfer is usually blurred by homonuclear *I-I* couplings, but it can be observed for certain systems and under suitable conditions (75) (see "Chemical Shift/Heteronuclear Coupling Correlations" below).

CP to dilute $S = \frac{1}{2}$ nuclei is usually carried out in combination with MAS for the sake of line narrowing. These could appear as conflicting procedures because the former is mediated by a heteronuclear coupling that the latter averages out (76). To appreciate why and how polarization can be transferred even under fast MAS it is illustrative to revisit the energy diagram originated by CP in the interaction frame introduced above (Figure 5*B*) (77): Spacings between the various $\{|IS\rangle = |M\alpha\rangle, |M\beta\rangle\}$ states are here defined by the ω^I_{rf}, ω^S_{rf} fields, homonuclear $\{\omega^{II}_D\} < \omega^I_{rf}$ couplings are responsible for a "spread" in these bands, and heteronuclear flip-flop terms enable an exchange and equilibriation of populations between $|M\alpha\rangle \leftrightarrow |(M+1)\beta\rangle$ manifolds.[15] Upon subjecting the sample to MAS—particularly to moderately fast spinning conditions—two distinctive changes will be introduced: $\pm\omega_r$ and $\pm 2\omega_r$ dependencies will be imparted on the heteronuclear couplings, and the width of homonuclear interactions will start scaling as $|\omega^{II}_D|/\omega_r$ (Figure 5*C*). As has been experimentally observed, the first of these changes modifies the secular transfer condition to $|\omega^S_{rf} - \omega^I_{rf}| = m\omega_r (m = \pm 1, \pm 2)$, whereas the second decreases the energy width of the $|IS\rangle$ manifolds and thus increases the accuracy with which these matching conditions need to be met (76, 78, 79). To deal with these complications a number of simple CP improvements have been proposed, including (*a*) changes in the *rf* levels of either *I* or *S* irradiation fields to enhance the chances of achieving an effective matching (80), (*b*) amplitude modulations of the ω_{rf} fields that involve adiabatic passages of the $\{|M\alpha\rangle, |(M+1)\beta\rangle$ manifolds and therefore a more effective exchange of their relative population (81, 82), and (*c*) repeated inversions in *rf* field phases in synchrony with reversals in the dipolar couplings (i.e. with the MAS process) (83).[16]

Cross Polarization to Half-Integer Quadrupoles

CP could also be potentially important for enhancing signals in quadrupolar NMR. Features that are relevant in an analytical context are the nature of CP to the sharper

[15] $\mathcal{H}^{IS}_D$ also contains double-quantum components that enable $|M\alpha\rangle \leftrightarrow |(M-1)\beta\rangle$ transitions. These terms govern the transfer when magnetization is spin-locked antiparallel to its *rf* field: *S* polarization is then generated antiparallel to B^S_{rf}.

[16] Driven by the emergence of sequences that will perform only suitably in the presence of very efficient proton decoupling, interest has also been spurred into finding the condition that minimizes the *I-S* CP transfer at the conclusion of a π_S pulse: $\omega^I_{rf}/\omega^S_{rf} = (2m+1)(m = 1, 2, \ldots)$ (84). This can place stringent decoupling conditions ($\omega^I_{rf} \geq 150$ kHz), particularly when *S* pulses much shorter than a rotor period and high ($\geq$8–10 kHz) MAS rates are desired. No similar anti-CP conditions have been found for $\pi/2_S$ pulses.

and easier to observe central transitions of half-integer $S \geq 3/2$ nuclei, and the possibility of combining CP with line-narrowing methodologies such as MAS. Because of the potentially large size of the quadrupolar interaction, its orientation dependence, and the presence of additional energy levels, the $S \geq 3/2$ scenario ends up being quite different from its spin-1/2 counterpart (85–87). The most evident difference concerns the nutation frequencies of the various transition: In the common $\omega_Q \gg \omega_{rf}^S$ limit these are $(S + 1/2)$ for the central transitions and $M\omega_{rf}^S(\omega_{rf}^S/\omega_Q)^{m-1}$ for other MQ transitions (with M a coefficient depending on the S and m numbers and ω_Q the Ω-dependent first-order effect).[17] It is this particular set of nutation rates that needs to be matched by ω_{rf}^I in order for the polarization of a particular transition to build up. For instance, when focusing on the central transition of a static powder, CP from a spin-1/2nucleus will occur between tilted spin-locked states

$$\gamma_I I_z \xrightarrow[\mathcal{H}_{IS}]{\omega_{rf}^I=(S+1/2)\omega_{rf}^S} \gamma_I (C_z/2)[1-\cos(\omega_D t)]/\left(S+1/2\right)+\cdots, \qquad 23.$$

where C denotes the central-transition fictitious spin-1/2 operator. This transfer looks similar to the one in Equation 22 except for the fact that only a fraction of I polarization, the portion associated with S's central transition, is actually getting transferred.

When executing MAS, this scenario changes owing to the periodic vanishing of the first-order quadrupole couplings for all crystallites in the powder. Indeed, large $\omega_Q \gg \omega_{rf}^S$ couplings justified neglecting the presence of satellite $m \leftrightarrow m-1$ transitions in the static case, but MAS will now force $\omega_Q(t)$ to vanish either two or four times per rotation period (depending on a single crystallite's orientation). At these zero-crossings ω_{rf}^S brings into contact all the states within the S-spin manifold (Figure 6), and polarization that had been transferred from I_z into C_z may redistribute into other spin populations and/or coherences. The actual fate of the spin-locked C_z will depend on a competition between the strengths of the first-order effect ω_Q separating central from satellite transition peaks, the ω_{rf}^S field recoupling these transitions, and the spinning rate ω_r controlling how long central and satellite transitions stay in contact during the zero-crossings. In fact, the outcome of these MAS-driven ω_Q modulations can be estimated from an analogy to the case of an *rf* field sweeping through the on-resonance condition of a spin-1/2 manifold (Figure 6*B*); in this scenario an S_z magnetization that was initially along B_o may end up parallel to $-z$ if the *rf* is swept slowly enough (adiabatic inversion), remain unchanged if the *rf* sweep is sudden, or begin to follow the effective field but end up in a non-spin-locked state (as coherences rather than populations) if the sweep rate is intermediate. The condition required from the

[17] In the opposite and rarely achievable limit $\omega_Q \ll \omega_{rf}^S$ the nutation frequencies for all 1Q transitions are equal and as in a spin-1/2 case, whereas for intermediate ranges several frequencies may arise simultaneously. Such complex behavior is the basis for 2D nutation NMR spectroscopy (88).

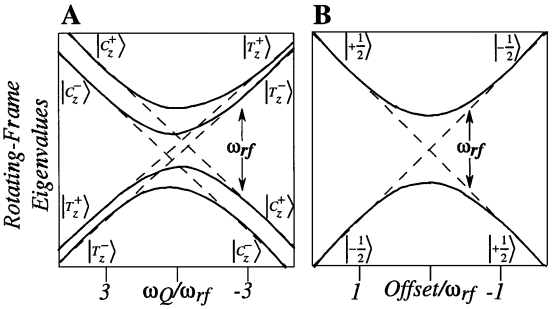

Figure 6 (*A*) Changes in the rotating-frame eigenvalues of a spin-$^3/_2$ arising from the oscillations imposed by magic-angle spinning on $\mathcal{H}_Q^{(1)}$. Two or four horizontal sweeps occur every T_R; depending on the rate of these changes states may interconvert (—, adiabatic passages), remain unchanged (---, sudden passages) or end up in non-spin-locked states (i.e. coherences that are not describable by this diagram). (*B*) Spin-$^1/_2$ analog of these effects, assumed to be driven by the sweep of an *rf* field through resonance.

changing $\gamma B_o(t)$ field for achieving adiabaticity during such a sweep is derived from the early literature (1): $\gamma \dot{B}_o \ll \omega_{rf}^2$. In the quadrupolar instance the first order $\omega_Q(t)$ takes the role of the $\gamma B_o(t)$ while the MAS-driven $e^{im\omega r^t}$ modulation defines the mechanism of the sweep; the condition for adiabatic transfer thus becomes $\omega_Q(t) \approx \omega_Q\omega_r \ll \omega_{rf}^2$. When this inequality is met each $\omega_Q \to 0$ zero-crossing will be associated with mutual exchanges between the spin-locked C_z populations and outer (e.g. $|^3/_2\rangle, |-^3/_2\rangle$) states; if this occurs while polarization is being transferred from I_z to C_z via CP, the net result is an enhancement of both central and MQ populations. On the other, sudden extreme ($\omega_{rf}^2 \ll \omega_Q\omega_r$), polarization transferred to the central transition remains unchanged during the crossing and CP thus proceeds as in the $S = ^1/_2$ case, except for the MAS- and quadrupole-modified $\omega_{rf}^I = (S + ^1/_2)\omega_{rf}^S \pm m\omega_r$ matching condition. This sudden-passage condition is easier to satisfy, yet to be truly valid for a majority of crystallites it may demand the use of very weak *rf* fields associated with short relaxation times and inefficient transfers. In many practical cases it is therefore the intermediate $\omega_Q\omega_r \approx \omega_{rf}^2$ regime that is satisfied by a majority of crystallites in a sample; each zero crossing then helps transform the spin-locked populations into single- and multiquantum coherences that rapidly decay and fail to contribute to observable signal, making CP particularly ineffective as a signal-enhancement technique.[18]

[18]Because of similar complications, many sophisticated multiple-pulse sequences developed for $S = ^1/_2$ cases may not be directly applied on half-integer quadrupoles. Alternatively, this rotationally induced dissipation serves as an efficient drain of the *I*-spin reservoir and can be used as an efficient spectral editing mechanism (see "Chemical Shift/Heteronuclear Coupling Correlations" below).

THE SELECTIVE REINTRODUCTION OF SPIN ANISOTROPIES

Avoiding the Penalties of High Resolution

The various manipulations described above may enable the acquisition of high resolution spectra endowed with good S/N, yet they do so at the expense of eliminating an orientation dependence that may otherwise have proven valuable. A practical solution to this information/resolution dichotomy is provided by 2D NMR, which can separate along a high-resolution spectral axis the rich but poorly resolved anisotropic information (4, 9, 13). In fact, some of the experiments described above (DAS, MQMAS) yield, by their very nature, isotropic/anisotropic 2D correlation spectra. Other such experiments that have been realized include pairwise correlations of isotropic and anisotropic shieldings (60, 89, 90), of shifts and dipolar couplings (91, 92), and of shifts and first-order $S = 1$ quadrupolar anisotropies (93, 94), as well as higher-dimensional correlations involving various triads of these interactions (95–97). For the sake of maximizing resolution a majority of these experiments encodes the isotropic evolution along the directly detected dimension; the anisotropic evolution that modulates individual peaks can then be extracted either by analyzing $S(t_1, \omega_2)$ time-domain functions or via a second transformation along the anisotropic domain. The two procedures are obviously related, but the former is usually preferred when trying to assess relatively small interactions such as the dipolar coupling between distant spins.

By virtue of the similar $\tilde{R}^{\lambda}_{20}(t)T^{\lambda}_{k0}$ dependencies that characterize all first-order anisotropies subject to sample spinning, there are certain common ways for reintroducing these couplings along an indirect t_1 domain. Conceptually the simplest is probably to spin the sample off-MAS (60), as then anisotropies are reintroduced with a scaling $d^{(2)}_{00}(\beta) \neq 0$.[19] This has been exploited in various applications, even if practical and S/N complications arise from the need to introduce a storage period in between t_1 and t_2 for the sake of rapid reorientation to (and subsequently during the relaxation delay, from) the magic angle. Such demands can be alleviated by replacing the correlated dynamic-angle evolution with a set of conventional variable-angle sample spinning acquisitions, followed by a simple interpolation of the data (99). An alternative to these fast-spinning spatial modulations is imposed by the magic-angle hopping and turning experiments (90, 100), which on the basis of repetitive storages on a slowly reorienting sample make $\langle \tilde{R}^{\lambda}_{20} \rangle = 0$ during the t_1 domain and correlate the ensuing isotropic evolution with a static-like anisotropic lineshape along ω_2.

The demands of these experiments for specialized instrumentation have stimulated the search for anisotropy-recoupling protocols that employ constant MAS

[19] Because the static spins' evolution is equivalent to that of a powder rotating at $\beta = 0^{\circ}$, a related procedure is to stop the sample MAS altogether during t_1; this is the basis for the "stop-and-go" 2D NMR experiment (98).

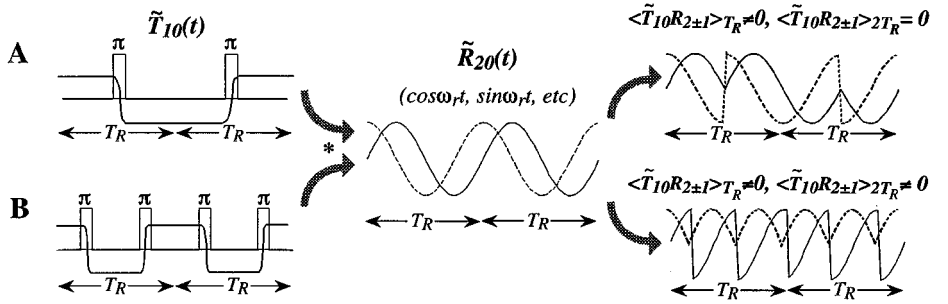

Figure 7 Reintroduction of the anisotropic interactions resulting from the synchronous modulation of spin ($\tilde{T}$) and spatial ($\tilde{R}$) terms in the coupling Hamiltonian. The cumulative behavior expected when using (*A*) one π-pulse/T_R and (*B*) two π-pulses/T_R is shown. Similar arguments can be extended to other coupling ranks and orders.

but spoil this averaging during t_1 via rotor-synchronized spin-space manipulations (89, 101). Making $\langle \tilde{R}^{\lambda}_{20}(t_1)\tilde{T}^{\lambda}_{k0}(t_1)\rangle_{\rm MAS} \neq 0$ is best visualized for the simplest case of an isolated spin subject to its local ω^{aniso}_{CS}. As described in Figure 3, MAS will refocus this anisotropy at every multiple of T_R, yet this averaging can be interrupted by the application of a π-pulse during the course of the rotor period (47). Magnetizations from different crystallites will then be taken away from their MAS trajectories, failing to refocus at $t = T_R$ and bringing about a signal decay that depends on the site's anisotropy.[20] Such dephasing can be understood as arising from a destructive interference between the spatial $\tilde{R}_{20}(t)$ and spin $\tilde{T}_{10}(t)$ terms of Hamiltonian (Figure 7), with the latter becoming time-dependent ($S_z \rightarrow -S_z$) in an interaction representation imposed by the π-pulse. A simple single-pulse/T_R approach cannot serve as the basis of pulse sequences that accumulate an anisotropic dephasing over evolution times $t_1 > \mathrm{T}_R$, as the application of a second π-pulse will undo the first pulse's effect (Figure 7*A*). Two π-pulses per T_R, on the other hand, can serve as useful rotor-synchronized anisotropic dephasing blocks (Figure 7*B*), even if the nature of the dephasing depends on the exact location of the pulses (103). Maximum dephasing will occur if these are spaced $T_R/2$ intervals apart, and the ideality of these experiments usually benefits from short ($\ll T_R$) pulse widths and from an *XY*-type of phase cycling (104). The lineshapes that result from Fourier analyzing these decaying signals carry anisotropic information but do not resemble static-like powder patterns; at least four π-pulses per rotor cycle are needed for obtaining such patterns within a measurable scaling factor (105).

[20] Effects similar to those introduced by π-pulses can be achieved by "freezing" the evolution of the spins during a fraction of T_R, using for instance, pairs of rotor-synchronized back-to-back $(2m\pi)_{\phi}(2m\pi)_{-\phi}$ nutation pulses (102).

Chemical Shift/Heteronuclear Coupling Correlations

As mentioned earlier, dipole-dipole anisotropies provide a convenient means for measuring internuclear distances. This task can be facilitated by the concurrent elimination of complicating local effects such as chemical-shift anisotropies, calling again for pulse sequences that will selectively preserve only one kind of interaction. A selective reintroduction of dipolar couplings is particularly straightforward for isolated heteronuclear spin-½ pairs via the spin-echo double resonance (SEDOR) experiment (11, 106)

$$\pi/2_S - t_1/2 - (\pi_1, \pi_S) - t_1/2 - \text{observe } S(t_1). \qquad 24.$$

When ideal π-pulses are involved the resulting $S(t_1)$ signals are solely a function of spin-relaxation and of the *I-S* dipolar coupling; normalization by $S_o(t_1)$ signals acquired in the absence of π_I pulses then leads to "universal" $\langle S/S_o \rangle (t_1)$ dephasing curves, depending solely on the dipolar couplings and from which *I-S* distances can be extracted.[21] Alternatively, SEDOR can be implemented as a full-fledged 2D experiment (in unison with homonuclear *I* decoupling if *I-I* couplings are a complication), resulting in "separate-local-field" signals $S(t_1, t_2)$ whose transforms correlate *S*'s dipolar and shielding anisotropies (107, 108). The nature of multiple *I-S* couplings (e.g. in I_mS systems) can also be analyzed via SEDOR if the π_I-pulse is replaced by a variable θ_I irradiation (109), and changes to the basic sequence may also enable its extension to quadrupolar nuclei [e.g. replacing the π_S-refocusing pulse by $\pi/2_S$ when $S = 1$ (110)]. Yet the most widespread SEDOR modifications are probably those introduced in an effort to merge this dipolar protocol with MAS as a means of enhancing the resolution and sensitivity of the *S* spectrum (111–114); we briefly turn to describing these experiments.

Perhaps the simplest dipolar/MAS conflict to resolve arises when trying to determine large spin-spin couplings such as those occurring in directly bonded ^{1}H-*S* systems; enough dipolar dephasing then occurs within one rotor period (or equivalently, enough intensity remains in the spinning sidebands of the separate-local-field spectrum) to require only minor rotor-synchronization modifications on the SEDOR protocol (115–117). The situation is different when trying to quantify *I-S* couplings between nonbonded and/or low-γ nuclei; here it may still be possible to rely on SEDOR-like sequences, provided that $\omega_D^{IS}(t)$ is actively reintroduced during t_1 periods extending beyond a single T_R. Because heteronuclear dipolar couplings transform as shielding anisotropies, any of the spatial and spin manipulation strategies discussed in the previous subsection of this article could be exploited for such ends. Most widespread among these are those variants relying on the application of two synchronized π-pulses per T_R, collectively known as rotational-echo double-resonance (REDOR; Figure 8) (111, 118). REDOR variants

[21] Carrying out such normalization has the important consequence of canceling to a large extent both residual local- as well as T_2-dephasings, enabling the estimation of dipolar couplings even when comparable or smaller than these effects.

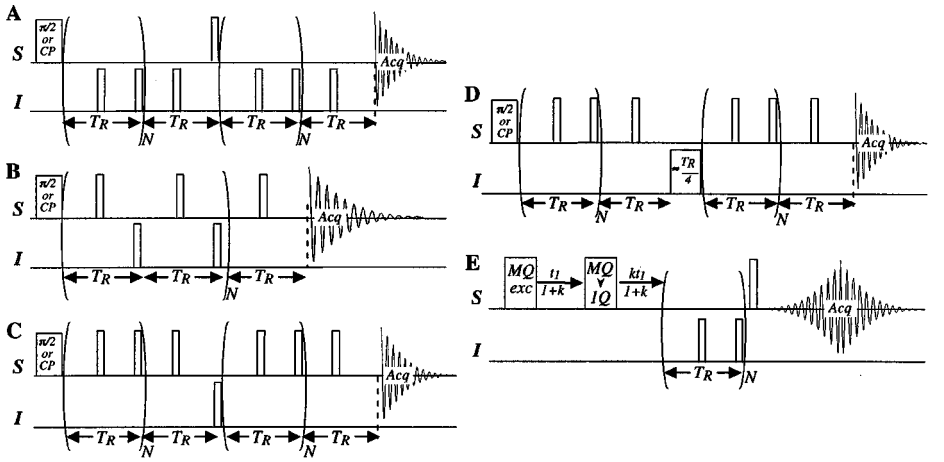

Figure 8 Recoupling alternatives for heteronuclear spin-½/spin-½ (*A–C*) or spin-½/quadrupole (*D, E*) distance measurements. (*A–C*) rotational-echo double-resonance (REDOR) variants; (*D*) rotational echo by adiabatic passage double resonance ($I \geq 1$); (E) MQMAS REDOR combination ($S \geq 3/2$). Unlabeled rectangles denote π-pulses whose phases are usually cycled to remove nonidealities.

arise from the fact that dipolar couplings transform as I_zS_z, and therefore dephasing can be achieved by placing all pulses at the *I* frequency, the *S* frequency, or alternating between the two. Placing all dephasing pulses on the *I* spins (Figure 8*A*) has the bonus of never incurring in a ω_{CS}^{aniso} dephasing of the *S* signal, yet it has been observed that for $I = S = 1/2$ the highest distance accuracies are generally achieved when alternating the dephasing pulses over the two channels (Figure 8*B*) (119). Because the effective *S* irradiation involved in this case is only one π-pulse per T_R, both isotropic and anisotropic *S* shieldings refocus after every other rotor period, making this the basic unit of t_1-incrementation.[22] Extracting long-range distances between heteronuclear spin-½ pairs also requires collecting a reference set S_o in the absence of π_I pulses, which is then employed for calculating $\langle S/S_o \rangle$ dephasing or $\langle (S_o - S)/S_o \rangle$ build-up curves. In principle, these depend solely on the dimensionless parameter $\lambda_D = \omega_D t_1 = m\omega_D T_R$, and therefore a single λ_D measurement could yield the desired distances. In practice, however, particularly if incomplete isotopic labeling might be involved, accuracy is increased by fitting whole portions of these curves. Direct numerical transforms are also available for extracting one or multiple ω_D values when these are sizable and the quality of the dephasing data is good (120).

A quantitative analysis on the effects of REDOR multiple-pulse trains becomes more challenging if one of the coupled species (*I*) is quadrupolar. Simplifying

[22] At least conceptually, practical increments are usually larger owing to the benefits resulting from XY-type phase cyclings of the *I*, *S* pulse trains.

conditions may arise when $\omega_{rf}^{I} > \omega_{Q}^{I}$ (potentially achievable for $I = {}^{2}\mathrm{H}$) (121) or when it can be assumed that only the I central transition has been manipulated, yet even in these cases it is advisable to apply the smallest possible number of pulses on the quadrupolar nucleus (Figure 8*C*). When the single $I_z \rightarrow -I_z$ reversal that then remains cannot be ensured by a π_I pulse, it may be preferable to forgo this scheme altogether and achieve a redistribution of I_z populations by exploiting the zero-crossing phenomena discussed above in relation to quadrupolar cross polarization MAS (122, 123). The rotational echo by adiabatic passage double resonance (REAPDOR) sequence has been derived on these principles (124); it employs an *I*-irradiation period placed at the center of the sequence and is timed so that a majority of crystallites in the sample experience a zero-crossing through resonance but are unlikely to have undergone two such exchanges (Figure 8*D*). A quantitative analysis of the ensuing *S*-decay still requires explicit spin propagations as well as knowledge of *I*'s quadrupolar tensor parameters, even if general "universal-like" curves may be proposed (125). S/N permitting, an alternative that enables a reversal to the simple REDOR-like dephasing analysis arises if the quadrupole nucleus is made the target of observation (Figure 8*E*). Experiments of this kind involving a MQMAS-driven refocusing of the quadrupolar anisotropies in combination with $I = {}^{1}/_{2}$ dephasing pulses have been demonstrated and shown to be amenable to interpretations involving solely the *I-S* dipolar interactions (126, 127).

The dipolar recoupling principles underlying REDOR can also find a role in the spectral assignment of complex systems. For instance, transferred-echo double-resonance (TEDOR), a dipole-based coherence transfer experiment applicable to both organic and inorganic systems (128, 129), can be used for simplifying spectra or assigning their resonances. Solution-like 2D heteronuclear correlations between $^{13}\mathrm{C}/^{15}\mathrm{N}$ and $^{13}\mathrm{C}/^{2}\mathrm{H}$ in isotope-labeled polycrystalline proteins have also been implemented on the basis of this protocol (Figure 9) (130, 131).

Though simple and efficient, rotor synchronized π-pulses are but one way of precluding the MAS averaging of heteronuclear dipolar couplings: given the $\omega_D(t) I_z S_z = \tilde{R}_{20}^{D}(t) T_{10}^{S} T_{10}^{I}$ form of this interaction, any manipulation that makes T_{10}^{λ} the periodically time dependent and can interact destructively with the $R_{2m} e^{im\omega_r t}$ terms in $\tilde{R}_{20}^{D}(t)$ will result in a recoupling. An example of this is rotary resonance recoupling (R^3) (132), which continuously irradiates I spins with a nutation frequency $\omega_{rf}^{I} = \omega_r$ or $2\omega_r$ and thus achieves $\langle \mathcal{H}_D(t) \rangle_{\mathrm{MAS}} \neq 0$ (see Equation 16).[23] Conceptually similar but more general forms of heteronuclear recoupling involving simultaneous frequency and amplitude modulations (SFAM) of the double-resonance (134), phase-cycled rotor-synchronized cycles (135), and nearly arbitrary forms of phase- and amplitude-modulated irradiation (136), have also been recently demonstrated.

[23] The effective $\mathcal{H}^{(1)}$ Hamiltonian also ends up dependent on *I*'s shielding anisotropy parameters, a complication that to some extent can be compensated by alternating the phase of the *rf* irradiation (133). R^3 also occurs in an increasingly weaker fashion if $(\omega_{rf}^{I} = m\omega_r)_{m \geq 3}$, by virtue of higher order AHT terms.

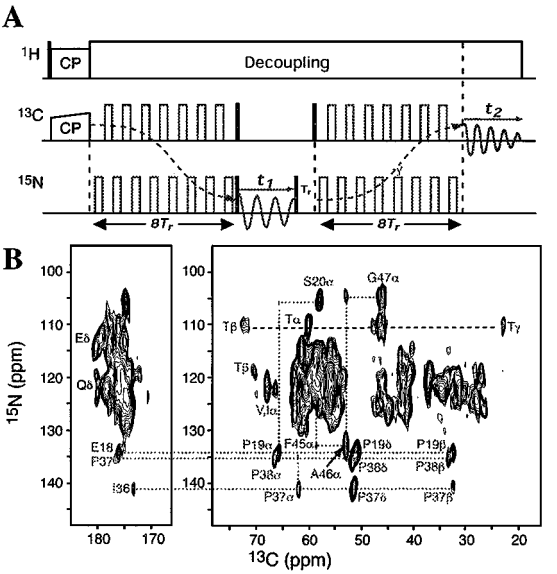

Figure 9 2D ^{15}N-^{13}C heteronuclear correlation experiment on ^{13}C-selectively/^{15}N-uniformly enriched ubiquitin. (*A*) Pulse sequence based on back-and-forth transferred-echo double-resonance coherence transfers, with thick lines and rectangles denoting $\pi/2$ and π pulses respectively. (*B*) Partial assignment of the resolved $^{13}C_{\alpha}$-^{15}N and ^{13}CO-^{15}N resonances. (Adapted from 169)

SEDOR is not the sole starting point for investigating heteronuclear couplings; the CP dynamics in Equation 22 in combination with homonuclear (frequency-shifted LG) decoupling and repetitive inversions of the *I* and *S* spin-temperature, also open up opportunities for accurate measurements of large coupling constants and serve as basis for the polarization-inversion with spin-exchange at the magic-angle (PISEMA) sequence (Figure 10) (137, 138). An alternative to these coherent *I*-*S* forms of recoupling is also offered by variants of the 2D exchange NMR technique in which the *S* magnetization is allowed to dephase under *I*'s dipolar field, stored over times $\tau \gg T_1^I$, and subsequently recalled and refocused into a stimulated echo (139). Random fluctuations in *I*'s spin state will lead to a dipole-encoding echo attenuation without having to irradiate the *I* spins, which for $I > 1/2$ cases can be made independent of quadrupole parameters (97).

Chemical Shift/Homonuclear Coupling Correlations

Equally important to the determination of molecular structures can be the measurement of distances between homonuclear *I*-*S* pairs under the presence of MAS. Yet the overall SEDOR strategy discussed in the preceding paragraph is complicated in these systems by at least two factors: the more complex nature of the dipolar

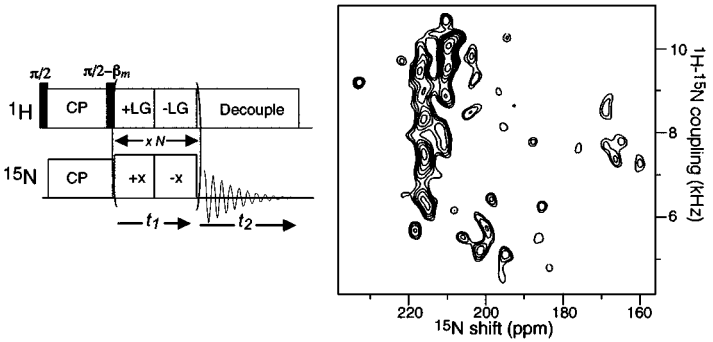

Figure 10 2D local-field polarization-inversion with spin-exchange at the magic-angle (PISEMA) spectrum of static ^{15}N-labeled fd bacteriophage viruses ($M_\omega \approx 16{\cdot}10^3$ kD) magnetically oriented in B_o at 60°C; dipolar couplings are encoded by the combined frequency-shifted LG/CP dephasing shown in the sequence. (Adapted from 170)

Hamiltonian (containing flip-flop terms) and the usual impossibility of manipulating the various coupled sites in the system independently from one another. These factors combine to make the net dipolar effects dependent on the spins' chemical shielding parameters, tensors that are interesting themselves but not necessarily known or being sought when looking for structural information. These factors also complicate the quantification of SEDOR-type S/S_o curves reflecting the spins' decay owing exclusively to dipolar effects, thus restricting the accuracy with which homonuclear distances can be evaluated. In view of these challenges, it is not surprising to encounter a more fluid scenario here than in the heteronuclear recoupling case (112–114, 140). This section provides a brief overview of some of its avenues.

The selective dephasing and rephasing π-pulses on which SEDOR and its daughter techniques rely are not directly applicable to homonuclear systems, as these will simultaneously affect the I and S spins and thereby have no effect on their mutual coupling. Still, a complete refocusing of the homonuclear evolution is possible provided that the heteronuclear π_I, π_S combination is replaced by a $\pi/2$ rotation; this is the principle of the solid-echo sequence (11, 141)

$$(\pi/2)_x - t_1/2 - (\pi/2)_y - t_1/2 - \text{observe } I + S \qquad 25.$$

which is strictly valid only when the two coupled spins are magnetically equivalent (no chemical shift differences). In analogy with the $T_{10} \rightarrow -T_{10}$ effects ascribed to π-pulses (Figure 7), the central $\pi/2$ pulse in this sequence can be thought of as having reversed the net effect of the homonuclear dipolar evolution. Consequently, replacing the π-driven modulation of REDOR with a similar train of rotor-synchronized $\pi/2$ pulses introduces a time dependence of the homonuclear dipolar coupling that prevents its spatial refocusing by MAS. This constitutes the basis for dipolar recovery at the magic angle (DRAMA; Figure 11*A*) (142, 143), a

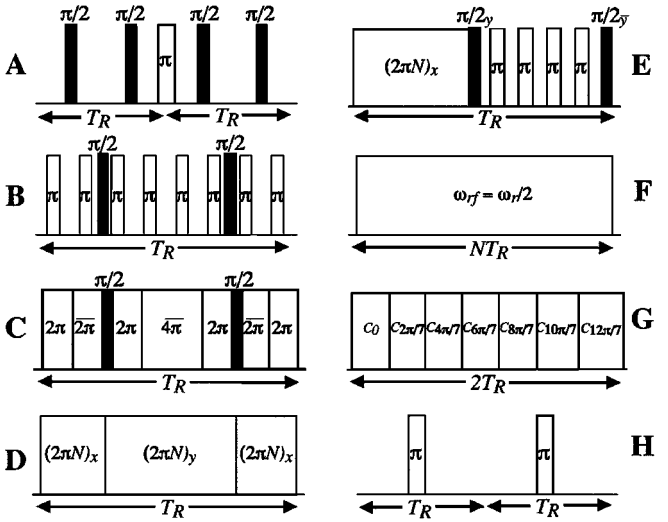

Figure 11 Alternatives for the rotor-synchronized, *rf*-driven recoupling of homonuclear spin-pairs under magic-angle spinning. In practical experiments these rotor-synchronized building blocks are usually further cycled to remove potential shielding/*rf* nonidealities.

sequence whose operation can best be visualized in a toggling frame in which the dipolar Hamiltonian oscillates between $\widetilde{\mathcal{H}}_{zz}^{IS}$ and $\widetilde{\mathcal{H}}_{yy}^{IS}$ every half rotor period.[24] DRAMA exhibits a high recoupling (i.e. fast dephasing) efficiency (140), yet its reliance on a purely dipolar scenario makes it sensitive to the *I* and *S* chemical shielding parameters. A number of sequences thus employ DRAMA as a basic recoupling scheme but tailor it to attenuate its dependence on chemical shifts. One such example is XY8-DRAMA, which introduces extensively phase-cycled π-pulses in between the $\pi/2$ nutations in order to refocus the chemical shielding effectively (Figure 11*B*) (144). Another alternative is the dipolar recovery with a windowless sequence (DRAWS) (Figure 11*C*) (145, 146), which replaces DRAMA's periods of free evolution with intervals of forced *rf* spin precessions built around 2π-pulses. Melding of spin-locking and DRAMA (MELODRAMA) (Figure 11*D*) is another offset-compensated variant that bypasses DRAMA's $\pi/2$ pulses altogether, preventing instead the MAS averaging by toggling $\widetilde{\mathcal{H}}_D^{IS}(t)$ between the two (*x*-*y*) rotating-frame transverse axes (147). Yet additional hybrid variations include switching the homonuclear evolution from the rotating to laboratory (R/L) frames every half rotor period, with offsets being compensated during

[24] A time dependence of $\widetilde{\mathcal{H}}_{\alpha\alpha}^{IS}(t) = R_{20}^{IS} T_{20}^{IS}(\alpha)$, $T_{20}^{IS}(\alpha) = 3I_\alpha S_\alpha - I \cdot S$, is exploited in the dipolar-averaging condition of all static-sample multiple-pulse sequences: $T_{20}^{IS}(x) + T_{20}^{IS}(y) + T_{20}^{IS}(z) = 0$ (2, 5). In DRAMA, however, these changes are made synchronous with MAS and therefore $\langle R_{20}^{IS}(t) T_{20}^{IS}(t) \rangle_{\mathrm{MAS}} \neq 0$.

the first of these intervals by continuous irradiation and during the second via trains of π-pulses (Figure 11*E*) (148, 149).

Heteronuclear recoupling alternatives other than REDOR can also be extended to the case of homonuclear spin pairs. One such opportunity is opened by R^3, whose homonuclear rotary resonance (HORROR) variant exploits the fact that both nuclei are now being irradiated in order to modify the recoupling condition to $\omega_{rf} = \omega_r/2$ (Figure 11*F*) (150). Because all spatial $\tilde{R}_{20}(t)$ components oscillate at $(\pm\omega_r, \pm 2\omega_r)$, such *rf*-driven nutation rates are in principle too slow for recoupling single-spin interactions like ω_{CS}^{aniso}, but fast enough for making $\langle \tilde{R}_{20}^{D}(t)\tilde{T}_{20}^{IS}(t)\rangle_{\mathrm{MAS}} \neq 0$.[25] An attractive feature of this approach is its dependence on the powder angles (β, γ) defining the orientation of the internuclear *I-S* vector in the rotor frame: Whereas in DRAMA derivatives these angles scale the effective recoupling as products of trigonometric functions (e.g. $\sin 2\beta \cos \gamma$), a phase-encoded dependence on the γ-angle ($\sin 2\beta e^{i\gamma}$) appears in HORROR. Consequently, when considered over a powdered sample, HORROR gives a more readily detectable decay of the recoupled spins' coherences.

Related to this continuous *rf*-driven homonuclear MAS recoupling but more immune to *rf* imperfections is the CN_n family of sequences (Figure 11*G*), which recouples the MAS-modulated Hamiltonian by concatenating N phase–shifted *rf* pulses throughout n consecutive rotor periods (151). This pulsing imparts a controlled time dependence on the spin-space components of the coupling and allows one to select, at least to first-order in AHT, particular $R_{2m}^{D}\, T_{2\mu}^{IS}$ combinations that are unique to the homonuclear *I-S* coupling. One of the shortest such solutions involves $N = 7$ pulses, $n = 2$ rotor periods, and *rf* phases ϕ_{rf} incremented by $2\pi/N$; only purely dipolar $R_{2\pm1}T_{2\pm2}$ terms survive such incrementation, and an effective zero-order Hamiltonian results that is analogous to the HORROR one except for a smaller scaling factor.[26] Further improvements on C7's shielding independence have been demonstrated by refining the actual pulses used to define each phase-shifted propagator (POST-C7) (152) or via supercycling combinations (CMR7) (153).

Either the DRAMA or the HORROR/C7 derivations can be thought of as having analogues in the heteronuclear scenario. Contrasting to this is rotational resonance (R^2), which prevents the MAS averaging of the *I-S* dipolar interaction simply by setting the spinning rate at an integer fraction of the isotropic chemical shift difference between the sites: $|\omega_{CS}^{I} - \omega_{CS}^{S}| = m \cdot \omega_r$ (154–156). How and why this condition achieves recoupling can be appreciated when factorizing the total two-spin Hamiltonian into a double-quantum contribution acting on the $\{|\alpha\alpha\rangle, |\beta\beta\rangle\}$ subspace of $\{|IS\rangle\}$, and a commuting zero-quantum Hamiltonian acting on $\{|\alpha\beta\rangle, |\beta\alpha\rangle\}$

[25] In practice this selective dipolar recoupling may be significantly affected by the chemical-shift offsets of the coupled sites and, as in many windowless sequences, by *rf* inhomogeneity.

[26] This time dependence $T_{20} \xrightarrow{C7} \Sigma_{\mu=-2}^{2} d_{\mu 0}^{(2)}(\beta_{rf}) e^{-i\mu\phi_{rf}} T_{2\mu}$ is to be compared with $T_{20} \xrightarrow{HORROR} \Sigma_{\mu=-2}^{2} d_{\mu 0}^{(2)}(\frac{\pi}{2}) e^{-i\mu\omega_{rf}t} T_{2\mu}$; in either case recoupling occurs by interference with the $\tilde{R}_{20}^{D}(t)$ in Equation 17, but the former scheme is more robust.

(112, 156, 157). A definition of operators

$$I_z^{\Delta} = \frac{1}{2}(|\alpha\beta\rangle\langle\alpha\beta| - |\beta\alpha\rangle\langle\beta\alpha|) = \frac{1}{2}(I_z - S_z);$$
$$I_x^{\Delta} = \frac{1}{2}(|\alpha\beta\rangle\langle\alpha\beta| - |\beta\alpha\rangle\langle\alpha\beta|) = \frac{1}{2}(I_+S_- + I_-S_+) \qquad 26.$$

enables one to express the latter contribution as a 2×2 irradiation-like Hamiltonian $\mathcal{H}_{\Delta} = \omega_{\Delta} I_z^{\Delta} + \omega_1 I_x^{\Delta}$, where the offset $\omega_{\Delta}(t)$ reflects the instantaneous difference between I and S chemical shifts, and $\omega_1 = \omega_D(t)$ is the time-dependent dipolar coupling. Upon MAS these longitudinal and transverse components average to the isotropic difference ω_{Δ}^{iso} and zero, respectively, thereby leading to a time evolution that is free from dipolar effects. Yet when any of the time dependencies modulating $\omega_D(t)$ match the average chemical shift difference ($\omega_{\Delta}^{iso} = \omega_r$ or $2\omega_r$) a resonance condition occurs within this 2×2 subspace, not unlike the one observed when the laboratory frame irradiation frequency of an *rf* field matches the spins' Larmor frequency. The evolution of an I^{Δ} vector under this rotational resonance condition will then reflect the strength of *I*-*S* dipolar couplings and enable their measurement.[27] Still, accurate long-range distance determinations by R^2 require additional a priori knowledge of the remaining parameters that affect the subspace evolution, including the *I* and *S* shielding tensors [which influence the instantaneous value of $\omega_{\Delta}(t)$] and the relaxation times of the zero-quantum vector. Methods have been proposed for independently measuring these quantities (158) as well as for alleviating the narrowness of the R^2 matching condition (159, 160). Furthermore, thanks to its relative simplicity, R^2 is one of the few recoupling mechanisms directly applicable to quadrupole nuclei (161).

By its very nature R^2 is a highly selective method for measuring homonuclear distances. An *rf*-driven, broadband alternative to the R^2 effect is offered by the simple excitation for the dephasing of rotational-echo amplitudes (SEDRA) protocol (162, 163), which achieves a broadband dipolar recoupling by applying one π-pulse per T_R (Figure 11*H*). SEDRA's dephasing principles can be gathered from considering the effects that its pulse train will have on the various *I*,*S* interactions within their zero-quantum subspace: The spin part of the homonuclear coupling will remain unaffected, the shielding anisotropy will dephase every odd but refocus every even rotor period (and thus it is to even multiples of T_R that dephasing increments will end up circumscribed), while isotropic shieldings will undergo periodic spin-echo time reversals. Such square-wave modulation of $\omega_{\Delta} I_z^{\Delta}$ every T_R can be viewed as effectively splitting the shift difference spectrum into a series of harmonics positioned at multiples of ω_r, and thus being susceptible to undergo R^2-type recoupling with $\omega_D(t)$ regardless of the sites' isotropic shift values. It also follows that in contrast to HORROR and DRAMA, SEDRA's dephasing is biased towards systems with sizeable ω_{Δ}^{iso} values, on the order of ω_r (140).

[27] ω_D will also influence I^{Δ}'s evolution when both sites have identical isotropic shifts ($m = 0$ R^2) or for $m \geq 3$ conditions, via weaker higher-order effects.

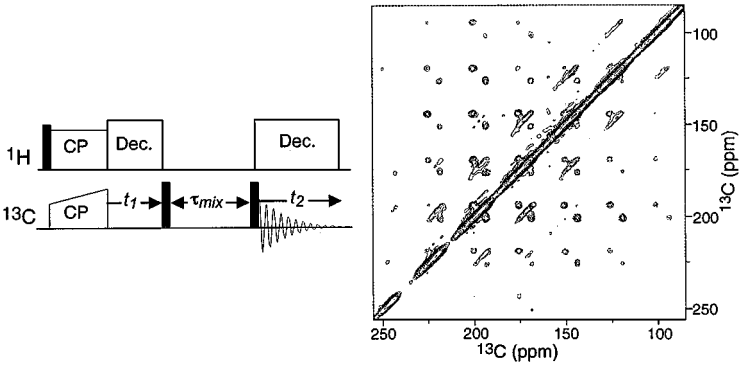

Figure 12 2D homonuclear ^{13}C correlation spectrum of a 24-residue HIV peptide, enriched at adjacent positions P320 and Gly321 and bound to a monoclonal antibody ($M_\omega >$ 50 kD); cross-peak intensities reveal the peptide's local conformation upon binding. Data were acquired using the spin-diffusion driven sequence on the left while executing MAS of a frozen solution at $-120°$C. (Adapted from 171)

As in the heteronuclear case, all these homonuclear recoupling sequences can be used to either introduce a dephasing that is directly monitored along a t_1 dimension or to activate couplings during the mixing periods of 2D chemical shift/chemical shift correlation experiment. Thanks to its simplicity and broad-bandedness, a SEDRA-derived scheme dubbed *rf*-driven recoupling (RFDR) has found the widest use for establishing this type of connectivity (113, 164), even if quantitative RFDR interpretations may be far from trivial when dealing with multiply-coupled networks (165). A peculiar feature of solid state homonuclear 2D correlations is that, given sufficiently long mixing times and often with the aid of a coupled proton network, dipolar-driven cross peaks between inequivalent sites may arise even in the absence of active *I-S* recoupling. These correlations are generated by spin-diffusion (166) and reflect the activity of flip-flop terms that have not been entirely truncated by MAS. The dynamics of these processes are slow (∼Hz) and not always amenable to quantitative kinetic analyses, yet in the complete exchange regime their resulting 2D lineshapes are featured and convey a clear picture of the relative geometry between the coupled sites (Figure 12) (167).

CLOSING REMARKS

Although limited in scope, it is hoped that the material summarized above conveys some of the progress that during recent years has characterized solid state NMR. Particularly encouraging has been the gradual inclusion of quadrupolar nuclei and of multiple-resonance distance determination techniques into the mainstream of experiments, as these have helped extend the frontiers of NMR as a spectroscopy while greatly improving its potential for the analysis of complex

solids. Notwithstanding this progress, important issues remain to be addressed in the field, including the development of new and simpler high resolution ^{1}H NMR protocols that can be incorporated into routine multidimensional experiments [an area that has already witnessed numerous advances (168)], additional heteronuclear decoupling improvements for furthering resolution, new signal enhancement approaches applicable to quadrupolar nuclei, and the reliable quantification of internuclear distances and angular constraints in multiply-labeled $I, S \geq 1/2$ systems. In view of the proven track record of breakthroughs and achievements in solids NMR, it is not so much a matter of if but of when and of how such targets will be achieved.

ACKNOWLEDGMENTS

It is a pleasure to acknowledge my many UIC-based co-workers for their insightful lessons and comments, as well as Ms. Rhonda Staudohar for her patient typing of manuscripts. This work was supported by the US National Science Foundation and Department of Energy, as well as by the Beckman, Dreyfus, University of Illinois, and Sloan Foundations.

LITERATURE CITED

1. Abragam A. 1961. *Principles of Nuclear Magnetism*. New York: Oxford Univ. Press
2. Haeberlen U. 1976. In *Advances in Magnetic Resonance*, ed. JS. Waugh, Suppl 1. New York: Academic
3. Spiess HW. 1978. In *NMR Basic Principles and Progress*, ed. P Diehl, E Fluck, R Kosfeld, 15:55–214. New York: Springer-Verlag
4. Fyfe CA. 1983. *Solid State NMR for Chemists*. Ontario: CFC Press
5. Mehring M. 1983. *High Resolution NMR in Solids*. Berlin: Springer-Verlag
6. Gerstein BC, Dybowski C. 1985. *Transient Techniques in NMR of Solids: An Introduction to Theory and Practice*. Orlando, FL: Academic
7. Derome AE. 1987. *Modern NMR Techniques for Chemistry Research*. Oxford: Pergamon
8. Munowitz MG. 1987. *Coherence and NMR*. New York: Wiley & Sons
9. Ernst RR, Bodenhausen G, Wokaun A. 1987. *Principles of Nuclear Magnetic Resonance in One and Two Dimensions*. Oxford: Clarendon
10. Goldman M. 1988. *Quantum Description of High Resolution NMR in Liquids*. New York: Oxford Univ. Press
11. Slichter CP. 1990. *Principles of Nuclear Magnetic Resonance*. New York: Springer-Verlag
12. McBrierty VJ, Packer KJ. 1993. *Nuclear Magnetic Resonance in Solid Polymers*. Cambridge, UK: Cambridge Univ. Press
13. Schmidt-Rohr K, Spiess HW. 1994. *Multidimensional Solid-State NMR and Polymers*. London: Academic
14. Stejskal EO, Memory JD. 1994. *High Resolution NMR in the Solid State: Fundamentals of CPMAS*. New York: Oxford Univ. Press
15. Blümich B, Kosfeld R, eds. 1994. *NMR:*

Basic Principles and Progress, Vols. 30–33. New York: Springer-Verlag
16. Grant DM, Harris RK, eds. 1996. *Encyclopedia of NMR*. Chichester, UK: Wiley & Sons
17. Cohen MH, Reif F. 1957. *Solid State Phys.* 5:321–48
18. Sakurai JJ. 1995. *Modern Quantum Mechanics*. Reading, MA: Addison-Wesley
19. Thayer AM, Pines A. 1987. *Acc. Chem. Res.* 20:47–56
20. Rose ME. 1995. *Elementary Theory of Angular Momentum*. New York: Dover
21. Haeberlen U, Waugh JS. 1968. *Phys. Rev.* 175:453–67
22. Freude D, Haase J. 1993. *NMR: Basic Princ. Progr.* 29:1–90
23. Maricq MM, Waugh JS. 1979. *J. Chem. Phys.* 70:3300–16
24. Chmelka BF, Zwanziger JW. 1994. *NMR: Basic Princ. Progr.* 33:79–123
25. Goldman M, Grandinetti PJ, Llor A, Oleniczak Z, Sachleben JR, Zwanziger JW. 1992. *J. Chem. Phys.* 97:8947–60
26. Shirley JH. 1965. *Phys. Rev. B* 138:979–1000
27. Vega S, Olejniczak ET, Griffin RG. 1984. *J. Chem. Phys.* 80:4832–40
28. Alderman DW, Solum MS, Grant DM. 1986. *J. Chem. Phys.* 84:3717–25
29. Smith SA, Levante TO, Meier BH, Ernst RR. 1994. *J. Magn. Reson. A.* 106:75–105. http://gamma.magnet.fsu.edu
30. Eden M, Lee YK, Levitt MH. 1996. *J. Magn. Reson. A.* 120:56–71
31. Hodgkinson P, Emsley L. 2000. *Prog. Nucl. Magnn. Reson. Spectrosc.* 36:201–39. http://www.durham.ac.uk/∼dch0ph/pubs
32. Bak M, Nielsen NC. 1997. *J. Magn. Reson.* 125:132–39. http://nmr.imsb.au.dk/simpson
33. Pines A, Gibby MG, Waugh JS. 1973. *J. Chem. Phys.* 59:569–90
34. Schaefer J, Stejskal EO. 1976. *J. Am. Chem. Soc.* 98:1031–32
35. Ernst M, Bush S, Kolbert AC, Pines A. 1996. *J. Chem. Phys.* 105:3387–97
36. vanderHart DL, Campbell GC. 1998. *J. Magn. Reson.* 134:88–112
37. Tekely P, Palmas P, Canet D. 1994. *J. Magn. Reson. A.* 107:129–33
38. Bennett AE, Rienstra CM, Auger M, Lakshmi KV, Griffin RG. 1995. *J. Chem. Phys.* 103:6951–58
39. Eden M, Levitt MH. 1999. *J. Chem. Phys.* 111:1511–19
40. Khitrin A, Fung BM. 2000. *J. Chem. Phys.* 112:2392–98
41. Lee M, Goldburg WI. 1965. *Phys. Rev.* 140:1261–65
42. Wang CH, Ramshaw JD. 1972. *Phys. Rev. B* 6:3253–60
43. Bielecki A, Kolbert AC, Levitt MH. 1989. *Chem. Phys. Lett.* 155:341–46
44. Hohwy M, Nielsen NC. 1997. *J. Chem. Phys.* 106:7571–86
45. Andrew ER, Bradbury A, Eades RG. 1958. *Nature* 182:1659
46. Lowe IJ. 1959. *Phys. Rev. Lett.* 2:285–87
47. Olejnizak ET, Vega S, Griffin RG. 1984. *J. Chem. Phys.* 81:4804–17
48. Herzfeld J, Berger AE. 1980. *J. Chem. Phys.* 73:6021–30
49. Jeschke G, Jansen M. 1998. *Angew. Chem. Int Ed. Engl.* 37:1282–83
50. Ermolaev K, Fung BM. 1999. *J. Chem. Phys.* 110:7977–82
51. Brunner E, Freude D, Gerstein BC, Pfeifer H. 1990. *J. Magn. Reson.* 90:90–99
52. Filip C, Hafner S, Schnell I, Demco DE, Spiess HW. 1999. *J. Chem. Phys.* 110:423–40
53. Ray S, Ladizhansky V, Vega S. 1998. *J. Magn. Reson.* 135:427–34
54. Zheng L, Fishbein KW, Griffin RG, Herzfeld J. 1993. *J. Am. Chem. Soc.* 115:6254–61
55. Isbester PK, Brandt JL, Kestner TA, Manson EJ. 1998. *Macromolecules* 31:8192–8200
56. Llor A, Virlet J. 1988. *Chem. Phys. Lett.* 152:248–53
57. Wooten EW, Mueller KT, Pines A. 1992. *Acc. Chem. Res.* 25:209–13

58. Samoson A, Lippmaa E, Pines A. 1988. *Mol. Phys.* 65:1013–18
59. Mueller KT, Sun BQ, Chingas GC, Zwanziger JW, Terao T, Pines A. 1990. *J. Magn. Reson.* 86:470–87
60. Bax A, Szeverenyi NM, Maciel GE. 1983. *J. Magn. Reson.* 55:494–97
61. Frydman L, Harwood JS. 1995. *J. Am. Chem. Soc.* 117:5367–68
62. Medek A, Harwood JS, Frydman L. 1995. *J. Am. Chem. Soc.* 117:12779–787
63. Amoureux JP, Fernandez C, Steuernagel S. 1996. *J. Magn. Reson.* A123:116–18
64. Amoureux JP, Fernandez C, Frydman L. 1996. *Chem. Phys. Lett.* 259:347–55
65. Brown SP, Wimperis S. 1997. *J. Magn. Reson.* 128:42–61
66. Wu G, Rovnyak D, Griffin RG. 1996. *J. Am. Chem. Soc.* 118:9326–32
67. Duer MJ, Stourton C. 1997. *J. Magn. Reson.* 124:189–99
68. Marinelli L, Medek A, Frydman L. 1998. *J. Magn. Reson.* 132:88–95
69. Kentgens APM, Verhagen R. 1999. *Chem. Phys. Lett.* 300:435–43
70. Larsen FH, Nielsen NC. 1999. *J. Phys. Chem. A* 103:10825–32
71. Madhu PK, Goldbourt A, Frydman L, Vega S. 2000. *J. Chem. Phys.* 112:2377–91
72. Vosegaard T, Florian P, Grandinetti PJ, Massiot D. 2000. *J. Magn. Reson.* 143: 217–22
73. Gan Z. 2000. *J. Am. Chem. Soc.* 122:3242–43
74. Hartmann SR, Hahn E. 1962. *Phys. Rev.* 128:2042–53
75. Müller L, Kumar A, Baumann T, Ernst RR. 1974. *Phys. Rev. Lett.* 32:1402–6
76. Stejskal EO, Scheafer J, Waugh JS. 1977. *J. Magn. Reson.* 28:105–12
77. Marks D, Vega S. 1996. *J. Magn. Reson A* 118:157–72
78. Sardashti M, Maciel GE. 1987. *J. Magn. Reson.* 72:467–74
79. Meier BH. 1992. *Chem. Phys. Lett.* 188:201–7
80. Peersen OB, Wu X, Kustanovich I, Smith SO. 1993. *J. Magn. Reson.* A104:334–39
81. Hediger S, Meier BH, Ernst RR. 1995. *Chem. Phys. Lett.* 140:449–56
82. Baldus M, Geurts DG, Hediger S, Meier BH. 1996. *J. Magn. Reson. A* 118:140–44
83. Wu X, Zilm KW. 1993. *J. Magn. Reson. A* 104:154–65
84. Ishii Y, Ashida J, Terao T. 1995. *Chem. Phys. Lett.* 246:439–45
85. Vega AJ. 1992. *J. Magn. Reson.* 96:50–68
86. Vega AJ. 1992. *Solid State NMR* 1:17–32
87. Baltisberger JH, Gann SL, Grandinetti PJ, Pines A. 1994. *Mol. Phys.* 81:1109–24
88. Jannsen R, Veeman WS. 1988. *J. Chem. Soc. Faraday Trans.* 84:3747–69
89. Bax A, Szeverenyi NM, Maciel GE. 1983. *J. Magn. Reson.* 51:400–8
90. Bax A, Szeverenyi NM, Maciel GE. 1983. *J. Magn. Reson.* 52:147–52
91. Stoll ME, Vega AJ, Vaughan RW. 1976. *J. Chem. Phys.* 65:4093–98
92. Waugh JS. 1976. *Proc. Natl. Acad. Sci. USA.* 73:1394–98
93. Blumler P, Jansen J, Blümich B. 1994. *Solid State NMR.* 3:237–40
94. Spaniol T, Kubo A, Terao T. 1997. *J. Chem. Phys.* 106:5303–16
95. Medek A, Sachleben JR, Beverwyk P, Frydman L. 1996. *J. Chem. Phys.* 104:5374–83
96. Hu JZ, Alderman DW, Pugmire RJ, Grant DM. 1997. *J. Magn. Reson.* 126:120–26
97. Sachleben JR, Beverwyk P, Frydman L. 2000. *J. Magn. Reson.* 144:330–42
98. Zeigler RC, Wind RA, Maciel GE. 1988. *J. Magn. Reson.* 79:299–306
99. Frydman L, Chingas GC, Lee YK, Grandinetti PJ, Eastman MA, et al. 1992. *J. Chem. Phys.* 97:4800–8
100. Gan Z. 1992. *J. Am. Chem. Soc.* 114: 8307–9
101. Yarim-Agaev Y, Tutunjian PN, Waugh JS. 1982. *J. Magn. Reson.* 47:51–56
102. Hong J, Harbison GS. 1993. *J. Magn. Reson. A* 105:128–36

103. Gullion T. 1989. *J. Magn. Reson.* 85:614–19
104. Gullion T, Baker DB, Conradi MS. 1990. *J. Magn. Reson.* 89:479–83
105. Tycko R, Dabbagh G, Mirau PA. 1989. *J. Magn. Reson.* 85:265–74
106. Emshwiller M, Hahn EL, Kaplan DE. 1960. *Phys. Rev.* 118:414–24
107. Linder M, Hohener A, Ernst RR. 1980. *J. Chem. Phys.* 73:4959–70
108. Terao T, Miura H, Saika A. 1986. *J. Chem. Phys.* 85:3816–22
109. Gullion T, Pennington CH. 1998. *Chem. Phys. Lett.* 290:88–93
110. Ba Y, Ratcliffe CI, Ripmeester JA. 1999. *Chem. Phys. Lett.* 299:201–6
111. Gullion T, Schaefer J. 1989. *Adv. Magn. Reson.* 13:57–83
112. Griffiths JM, Griffin RG. 1993. *Anal. Chim. Acta.* 283:1081–1101
113. Bennett AE, Griffin RG, Vega S. 1994. See Ref. 15, 33:3–77
114. Dusold S, Sebald A. 2000. *Ann. Rep. NMR Spectrosc.* 41:185–264
115. Munowitz MG, Griffin RG, Bodenhausen G, Wang TH. 1981. *J. Am. Chem. Soc.* 103:2529–33
116. Munowitz MG, Griffin RG. 1982. *J. Chem. Phys.* 76:2848–58
117. Schaefer J, McKay RA, Stejskal EO, Dixon WT. 1983. *J. Magn. Reson.* 52: 123–29
118. Gullion T, Schaefer J. 1989. *J. Magn. Reson.* 81:57–83
119. Garbow JR, Gullion T. 1992. *Chem. Phys. Lett.* 192:71–76
120. Mueller KT. 1995. *J. Magn. Reson. A* 113:81–93
121. Schmidt A, McKay RA, Schaefer J. 1992. *J. Magn. Reson.* 96:644–50
122. Grey CP, Veeman WS. 1992. *Chem. Phys. Lett.* 192:379–85
123. Grey CP, Veeman WS, Vega AJ. 1993. *J. Chem. Phys.* 98:7711–24
124. Gullion T. 1995. *Chem. Phys. Lett.* 246:325–30
125. Ba Y, Kao HM, Grey CP, Chopin L, Gullion T. 1998. *J. Magn. Reson.* 133:104–14
126. Fernandez C, Lang DP, Amoureux JP, Pruski M. 1998. *J. Am. Chem. Soc.* 120:2672–73
127. Pruski M, Bailly A, Lang DP, Amoureux JP, Fernandez C. 1999. *Chem. Phys. Lett.* 307:35–40
128. Hing AW, Vega S, Schaefer J. 1993. *J. Magn. Reson. A* 103:151–62
129. Fyfe CA, Wong-Mong KC, Huang Y, Grondey H, Mueller KT. 1995. *J. Phys. Chem.* 99:8707–16
130. Hong M, Griffin RG. 1998. *J. Am. Chem. Soc.* 120:7113–14
131. Sandström D, Hong M, Schmidt-Rohr K. 1999. *Chem. Phys. Lett.* 300:213–20
132. Oas TG, Levitt MH, Griffin RG. 1988. *J. Chem. Phys.* 89:692–95
133. Costa PR, Gross JD, Hong M, Griffin RG. 1997. *Chem. Phys. Lett.* 280:95–103
134. Fu R, Smith SA, Bodenhausen G. 1997. *Chem. Phys. Lett.* 272:361–69
135. Gross JD, Costa PR, Griffin RG. 1998. *J. Chem. Phys.* 108:7286–93
136. Ishii Y, Terao T. 1998. *J. Chem. Phys.* 109:1366–74
137. Wu CH, Ramamoorthy A, Opella SJ. 1994. *J. Magn. Reson. A* 109:270–72
138. Ramamoorthy A, Gierasch LM, Opella SJ. 1996. *J. Magn. Reson. B* 110:102–6
139. Sachleben JR, Frydman V, Frydman L. 1996. *J. Am. Chem. Soc.* 118:9786–87
140. Baldus M, Geurts DG, Meier BH. 1998. *Solid State NMR* 11:157–68
141. Powles JG, Mansfield P. 1962. *Phys. Rev. Lett.* 2:58–61
142. Tycko R, Dabbagh G. 1990. *Chem. Phys. Lett.* 173:461–65
143. Tycko R, Smith SO. 1993. *J. Chem. Phys.* 98:932–43
144. Klug CA, Zhu W, Merritt ME, Schaefer J. 1994. *J. Magn. Reson. A* 109:134–36
145. Gregory DM, Mitchell DJ, Stringer JA, Kiihne S, Shiels JC, et al. 1995. *Chem. Phys. Lett.* 246:654–63

146. Kiihne S, Mehta MA, Stringer JA, Gregory DM, Shiels JC, Drobny GP. 1998. *J. Phys. Chem. A* 102:2274–82
147. Sun BQ, Costa PR, Kosisko D Jr, Lansbury PT, Griffin RG. 1995. *J. Chem. Phys.* 102:702–7
148. Fujiwara T, Ramamoorthy A, Nagayama K, Hioka K, Fujito T. 1993. *Chem. Phys. Lett.* 212:81–84
149. Baldus M, Tomaselli M, Meier BH, Ernst RR. 1994. *Chem. Phys. Lett.* 230:329–36
150. Nielsen NC, Bildsoe H, Jakobsen HJ, Levitt MH. 1994. *J. Chem. Phys.* 101: 1805–2
151. Lee YK, Kurur ND, Helmle M, Johannessen OG, Nielsen NC, Levitt MH. 1995. *Chem. Phys. Lett.* 242:304–9
152. Hohwy M, Jakobsen HJ, Eden M, Levitt MH, Nielsen NC. 1998. *J. Chem. Phys.* 108:2686–94
153. Rienstra CM, Hatcher ME, Mueller LJ, Sun BQ, Fesik SW, Griffin RG. 1998. *J. Am. Chem. Soc.* 120:10602–612
154. Colombo MG, Meier BH, Ernst RR. 1988. *Chem. Phys. Lett.* 146:189–96
155. Raleigh DP, Levitt MH, Griffin RG. 1988. *Chem. Phys. Lett.* 146:71–76
156. Levitt MH, Raleigh DP, Creuzet F, Griffin RG. 1990. *J. Chem. Phys.* 92: 6347–64
157. Gan ZH, Grant DM. 1990. *Mol. Phys.* 67:1419–30
158. Karlsson T, Levitt MH. 1998. *J. Chem. Phys.* 109:5493–5507
159. Costa PR, Sun B, Griffin RG. 1997. *J. Am. Chem. Soc.* 119:10821–30
160. Verel R, Baldus M, Nijman M, vanOs JWM, Meier BH. 1997. *Chem. Phys. Lett.* 280:31–39
161. Nijman M, Ernst M, Kentgens APM, Meier BH. 2000. *Mol. Phys.* 98:161–78
162. Gullion T, Vega S. 1992. *Chem. Phys. Lett.* 194:423–28
163. Weintraub O, Vega S, Hoelger C, Limbach HH. 1994. *J. Magn. Reson A* 109:14–25
164. Bennett AE, Ok JH, Griffin RG, Vega S. 1992. *J. Chem. Phys.* 96:8624–27
165. Hodgkinson P, Emsley L. 1999. *J. Magn. Reson.* 139:46–59
166. Meier BH. 1994. In *Advances in Magnetic and Optical Resonance*, ed. WS Warren, 18:1–116. New York: Academic
167. Weliky DP, Tycko R. 1996. *J. Am. Chem. Soc.* 118:8487–88
168. Hafner S, Spiess HW. 1998. *Concepts Magn. Reson.* 10:99–128
169. Hong M. 1999. *J. Magn. Reson.* 139:389–401
170. Tan WM, Zelink R, Opella SJ, Malik P, Terry TD, Perham RN. 1999. *J. Mol. Biol.* 286:787–96
171. Weliky DP, Bennett AE, Zvi A, Anglister J, Steinbach PJ, Tycko R. 1999. *Nat. Struct. Biol.* 6:141–45